Effects of Blockiness and Polydispersity on the Phase Behaviour of non-Markovian Random Block Copolymers

EFFECTS OF BLOCKINESS AND POLYDISPERSITY ON THE PHASE BEHAVIOUR OF NON-MARKOVIAN RANDOM BLOCK COPOLYMERS

BY

GORDON VANDERWOUDE, B.Sc.

A THESIS

SUBMITTED TO THE DEPARTMENT OF PHYSICS & ASTRONOMY

AND THE SCHOOL OF GRADUATE STUDIES

OF MCMASTER UNIVERSITY

IN PARTIAL FULFILMENT OF THE REQUIREMENTS

FOR THE DEGREE OF

MASTER OF SCIENCE

Master of Science (2016) McMaster University

(Physics & Astronomy) Hamilton, Ontario, Canada

TITLE:	Effects of Blockiness and Polydispersity on the Phase Behaviour of non-Markovian Random Block Copolymers
AUTHOR:	Gordon Vanderwoude B.Sc., (Physics) McMaster University, Hamilton, Canada
SUPERVISOR:	Dr. An-Chang Shi
NUMBER OF PAGES:	x, 96

Abstract

A model of non-Markovian random block copolymers is developed and used to study the effects of blockiness and compositional polydispersity on the phase behaviour of random block copolymers. The model approximates a random copolymer as a series of segments with equal lengths, while each segment is composed of sequences of different monomers drawn randomly from a distribution. The phase behaviour of the model random copolymers is first examined using the random phase approximation (RPA) to study the effects of blockiness and polydispersity on the order-disorder transition. It is observed that the critical point is inversely proportional to the blockiness. Compositional polydispersity is found to facilitate phase separation, and could induce macrophase separation. Next, the model is implemented into self-consistent field theory (SCFT) in order to elucidate the full phase behaviour of symmetric $A/B-A$ random copolymers. Finally, the model is applied to the particular case of poly(styrenesulfonate-b-methylbutylene) (PSS-PMB) to study the effects of blockiness on the phase behaviour. In particular, the stability and structure of the 'swollen gyroid' morphology predicted by previous Monte Carlo simulations is examined.

Acknowledgements

I would like at this moment to thank some of the many people who have supported me throughout my time of study at McMaster University. First and foremost, I would like to thank my mom Armeda Vanderwoude and my grandmother Betty Reade for their unflagging encouragement over the past seven years. I would also like to thank the congregation of Lowville United Church for their friendship and support during my years as their Organist and Music Director, with particular thanks to Dianne Segsworth, David Jerome, and Connie and Allan Salmi. I am also grateful to the congregation of Lift Church (McMaster) for their friendship and spiritual support over the past year, with particular thanks to Robin Wallar, and Emily and Matt Litow.

This work was made possible by the continued support and advice of my supervisor, Dr. An-Chang Shi. His guidance (and at times, patience) is sincerely appreciated. I am also grateful to my colleagues for our many useful and interesting discussions, with particular thanks to Ashkan Deghan, who taught me many of the numerical methods employed in this thesis.

Contents

List of Figures

Chapter 1

Introduction

The ability of block copolymers to spontaneously self-assemble to form a variety of ordered phases has made these systems an attractive topic of study, both for the interesting physics that they display and for the many potential applications utilizing their unique material properties. A polymer is a long chain molecule consisting of repeating subunits called monomers. A polymer in which all the monomers are identical is called a homopolymer. A block copolymer is a polymer composed of two or more monomer types, where 'block' refers to an uninterrupted sequence of identical monomers. For example, a diblock copolymer is a polymer consisting of a block of A monomers covalently bonded at one end to a block of B monomers (Figure 1.1).

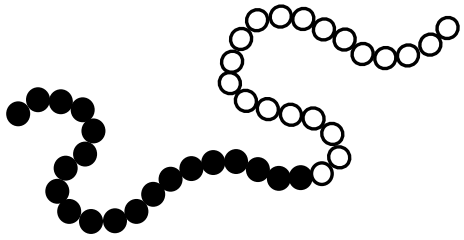

Figure 1.1: schematic of an AB diblock copolymer.

If the interactions between the different types of monomers are repulsive, the immiscible components would naturally tend to separate from each other. This enthalpically driven phase separation is opposed by the reduction in entropy due to the separation of the molecules. If the system was a blend of A and B homopolymers, the system would undergo a macroscopic phase separation, like oil and water. If the system is a melt of diblock copolymers the immiscible components are now in a frustrated state, unable to completely phase separate due to the chemical bond linking the two blocks. In such a situation, the system can reduce its free energy by microphase separating into a periodic nanostructure (Figure 1.2). The morphology of this ordered state is determined by the strength of the interactions, typically quantified by the Flory-Huggins parameter χ_{AB}; and the architecture of the chain. If the interactions are too weak or if the temperature is too high, the system may not phase separate at all and will remain in a disordered (or homogeneous) state.

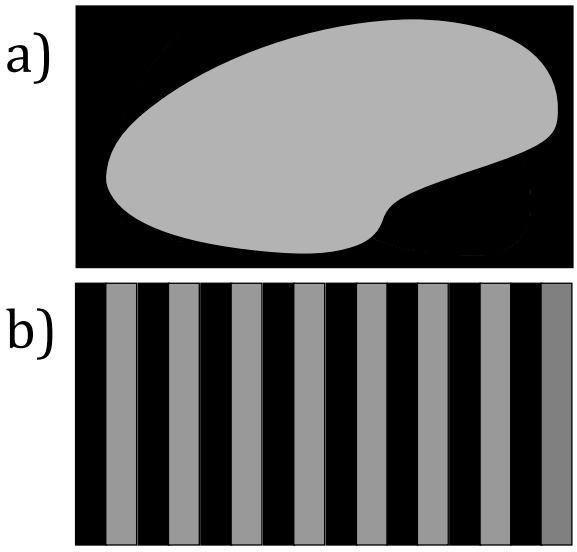

Figure 1.2: a) macrophase separated polymer melt into A-rich and B-rich domains. b) microphase seapration block copolymer melt into a periodic lamellar phase.

Variations in chain architecture are virtually unlimited, particularly if more than two monomer-types are included. In addition to purely linear polymers, there exist star polymers, branched polymers, comb polymers, and dendrimers, among others (Figure 1.3). Exploring the complete parameter space of a particular class of block copolymer can be an enormous undertaking [1]. If we assume that the chains are monodisperse (i.e. they are identical in length and monomeric sequence), the parameter space of a diblock copolymer melt is two dimensional. These independent variables are the enthalpic interaction $\chi_{AB}N$ and the relative lengths of the A and B blocks (often labelled f_A, which ranges from 0 to 1). Here N is the degree of polymerization. If we move one step up in complexity, and turn the AB diblock copolymer into an ABC linear triblock copolymer, the parameter space is now five dimensional, with three interaction parameters, and two independently adjustable block lengths. Due to the sheer enormity of the parameter space, for all but the simplest block copolymer architectures the elucidation of the complete phase behaviour is a formidable task.

Further levels of complexity can be introduced by relaxing the assumption of monodispersity. This variability, called polydispersity, can appear in two ways. One way is where the monomer sequence of the polymers is well controlled, but there is some variability in the actual lengths of the blocks. In real block copolymer melts, some degree of polydispersity of this kind will always exist, even when perfect uniformity is the goal. The other way is where the monomer sequence is not directly controlled, but is the result of some statistical process. In these systems, the sequence of each polymer is unique, and the uniformity of total monomer composition cannot be assumed. For many random copolymer melts, their sequences could be characterized by a Markov process. Briefly stated, a Markov process is a stochastic

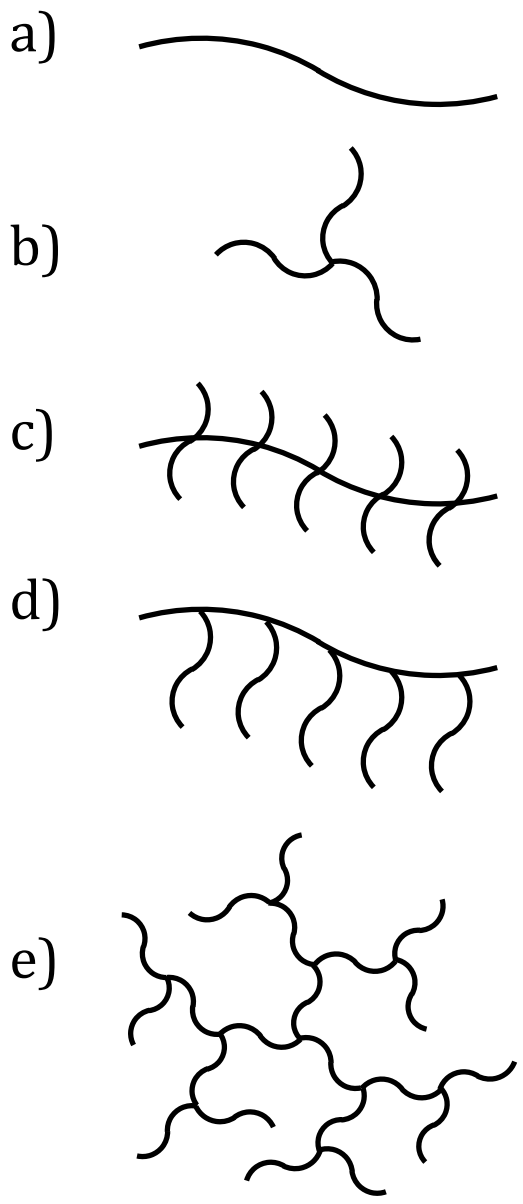

Figure 1.3: Examples of possible polymer architectures: a) linear, b) star, c) bottle-brush, d) comb, e) dendrimer.

process where each step depends only on its immediate prior state. The process that gives rise to a random copolymer is Markovian if the probably of adding an A or B monomer depends only on the type of the last monomer added (Figure 1.4). This process can be parametrized by 'pairing probabilities', which are the probabilities of every possible step: A following A, B following A, A following B, or B following B. Physically, these probabilities are determined by the competing reaction rates of polymerization and the relative abundance of the different monomer types available to the polymerization process. There also exist more specialized types of randomness, where the paring probabilities change as we move along the contour of the chain. These would include gradient, tapered, and inverse-tapered sequences. Indeed, there is such a variety of non-deterministic polymeric sequences within current technical capabilities, that the usual nomenclature is being stretched to its limits [2].

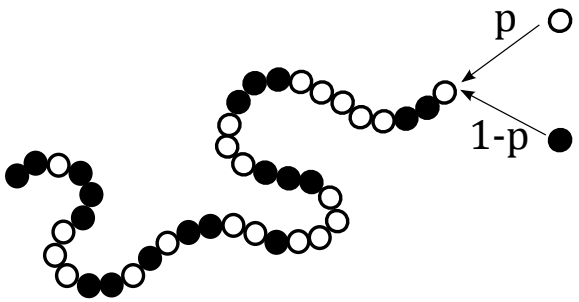

Figure 1.4: Schematic of a random copolymer being polymerized according to a Markov process. The probabilies of 'like' and 'unlike' pairings are p and $1-p$ respectively.

Significant theoretical work has been carried out in the study of the aforementioned Markovian random copolymers. [3, 4, 5]. These models allow the phase space to be defined succinctly. If the system contains only two monomer types A and B, the entire system is characterized by the interaction parameter χ_{AB} and a matrix of

pairing probabilities,

$$\begin{bmatrix} p_{AA} & p_{AB} \\ p_{BA} & p_{BB} \end{bmatrix}.$$

The phase space can be made two-dimensional by only considering 'like' and 'unlike' parings, and letting $p_{AA} = p_{BB} = p$ and $p_{AB} = p_{BA} = 1 - p$. Although incorporating the probability parameter p into the theoretical tools of polymer physics is not an easy task, these models have the great conceptual advantage of having an intuitively defined sequence space which is easily parametrizable. However, not all random copolymers can be defined in this way. There are cases where the paring probabilities change as a function of contour position, such as gradient copolymers, and there are random copolymers that cannot be described by Markov statistics at all. These would include polymers whose sequence is the result of post-polymerization treatments. One example would be poly(styrenesulfonate-b-polymethylbutylene) (PSS-PMB) in which a random selection of the polystyrene (PS) monomers are sulfonated, post-polymerization [6]. When studying the phase behaviour of non-Markovian random copolymers, the first problem is the issue of defining the sequence space. Although any sequence is technically possible, not all sequences are equally probable. It is necessary to have some way of quantifying the probability of a given sequence. Addressing this problem is the main work of this thesis.

Although the sequences are random, if they are all the product of the same process, they are all random 'in the same way'. As such, there should be certain general characteristics that differentiate one melt of random copolymers from another. One of these characteristics is the 'blockiness', which qualitatively could be thought of as a measure of how mixed the different monomer components are, along the contour of

a typical chain in the melt. This quantity, which will be defined quantitatively in the next chapter, will be the foundation of our model of non-Markovian random block copolymers. While the Markovian models are generally built from the 'bottom-up', starting from the chemistry of the polymerization process, we choose in our model to use a 'top-down' approach. The blockiness is used as a fundamental parameter from which a deterministic approximation of the system could be formulated. Starting from this deterministic approximation, we introduce randomness into it systematically.

Our model, which we call a Segment Model of Random Block Copolymers, treats each chain as composed of a series of equal-length segments whose individual sequences are drawn from a distribution. The number of sequences per chain, as well as the choice of sequence ensemble, allows for the systematic study of different kinds of randomness and chain architectures on the phase behaviour. In this thesis, we use the model to study the effects of three general characteristics of random copolymers: blockiness, compositional polydispersity, and sequential polydispersity. It is seen that blockiness is the dominant determiner of the phase behaviour but that compositional polydispersity can have a significant effect. On the other hand, sequential polydispersity, even if quite large, is seen to be relatively insignificant in its effects.

First, the order-disorder transition (ODT) is examined using the random phase approximation (RPA), which is used to calculate the order-disorder spinodal. The spinodal is the locus of points for which the second derivative of the Gibbs free energy is zero. This condition defines the limit at which the disordered state is unstable to small fluctuations. Past the spinodal, fluctuations from the disordered state ultimately lead to phase separation. In implementing the model in the RPA, it is shown that the computational cost of the calculation is independent of the dimensionality

of the sequence space. This means that the spinodal of random copolymer melts of almost arbitrary complexity can be calculated exactly.

The model is next implemented into self-consistent field theory (SCFT), which allows for the construction of complete phase diagrams. In this case, the dimensionality of the sequence space is an unavoidable obstacle. For situations in which the calculation cannot be done in full, different approximation methods are discussed. The SCFT implementation, in conjunction with the RPA implementation, is then used to describe the full phase behaviour of $A/B-A$ random copolymers. The results provide evidence that in the case of low compositional polydispersity, a deterministic approximation of the melt may be sufficient, even if the sequential polydispersity is large.

Finally, the model is used to study the phase behaviour of the aforementioned PSS-PMB and the results are compared to Monte Carlo (MC) simulations of this system. In particular, the structure of the 'swollen gyroid' morphology predicted by MC simulation and observed in experiment is examined. It is seen that this structure is stable for only the blockiest sequences, indicating the phase separation within the random PS/PSS block is a key to its stability. A close examination of the structure indicates that the swollen gyroid may be better described as a core-shell gyroid morphology with PSS channels embedded in a PS sub-matrix.

Chapter 2

Segment Model of Random Multiblock Copolymers

Much of the currently existing theory of random copolymers has been developed in the context of a Markov process, the statistics of which are determined by the competing reaction rates of polymerization. Random copolymers with non-Markovian sequences pose different challenges, since the sequence space and associated probability distribution are not easily defined. For example, suppose an A homopolymer is treated post-polymerization so that some of the A monomers are now B. Without knowing the details of the process, there is little that can be said *a priori*. Such details include the typical correlation of the B monomer concentration along a chain (the blockiness) and how evenly distributed are the B monomers amongst all the chains (the compositional variance). Our model, which we call a Segment Model of Random Copolymers, uses 'blockiness' as the fundamental parameter. Blockiness is defined as the average block lengths within the random sequences, scaled by the degree of polymerization. Quantitatively the blockiness provides a measure of how mixed the

monomer components are within the sequences.

To begin, we consider a random copolymer composed of A and B monomers, whose average block lengths are l_A and l_B, respectively. As a first approximation, we could regard all the polymers as identically alternating block copolymers, where each block has length l_A or l_B. Taking each pair as a single unit, we can define the blockiness as $b = \frac{l_A+l_B}{N}$. As such, the alternating copolymer can also be thought of as series of equal length diblocks, each with composition $f_A = l_A/b$. While this crude model may capture some of the general features of the system, the randomness of the monomer distribution along the chains is completely ignored.

One way to improve this simple approach is to model the polymers as a series of diblocks with equal length but variable compositions (Figure 2.1). Let f_A be the total monomer composition of the entire system. We can approximate each chain as a series of equal-length diblocks where the composition of each diblock is drawn from a distribution, chosen so that the average composition is f_A. Modelling a random block

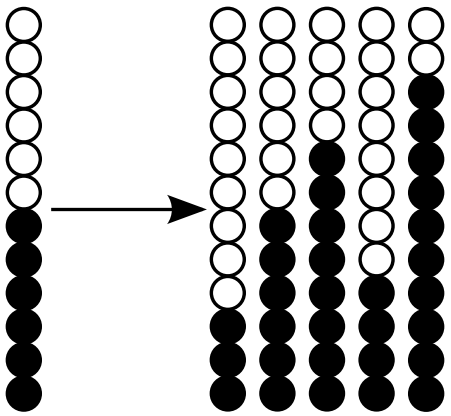

Figure 2.1: Schematics of the segments used in the model. The simplest model uses one type of diblock as the segments, whereas a more accurate model uses a number of diblocks with equal lengths but different block compositions drawn from a given distribution.

copolymer as a sequence of diblocks is just one approach. It is possible to use more complex segments, such as triblocks or multiblocks. A similar approach has been previously used to model gradient copolymers. Specifically, gradient copolymers were modelled as a series of equal length diblocks whose individual compositions decreased gradually from one end of the chain to another [7, 8]. It should be noted that in that particular case, the number of segments used was a matter of accuracy. The smaller the individual segments, the more continuous the gradient profile appears. In our model, the number of segments is chosen to control the blockiness. The less segments used, the blockier the profiles are.

We define an ensemble of sequences described by a set of profiles $g_\alpha(n, s)$ defined for $0 \leq s \leq 1$. Specifically, $g_\alpha(n, s)$ is the local concentration of α-type monomers at contour position s. n is an indexing parameter. The particular indexes are drawn randomly from a distribution $P(n)$. The model approximates each chain by M segments, each with a randomly selected set of profiles $g_\alpha(\{n\}, s)$ (Figure 2.2). There are only two restrictions, which will be important for later development: 1) each segment is of equal length and 2) the index parameters $\{n\}$ are independent of one another. It is assumed that all the segments are drawn from the same distribution, though this is not a requirement of the model, and will be relaxed in later chapters. Because the blockiness is defined as the average block lengths scaled by the length of the chain, within our model this quantity is inversely proportional to the number of segments used to the model the chain. This model suggests an alternative definition of blockiness, $b = \frac{1}{M}$.

In summary, the model is completely described by three factors: the number of segments M, which determines the blockiness ($b = M^{-1}$); the segment profiles

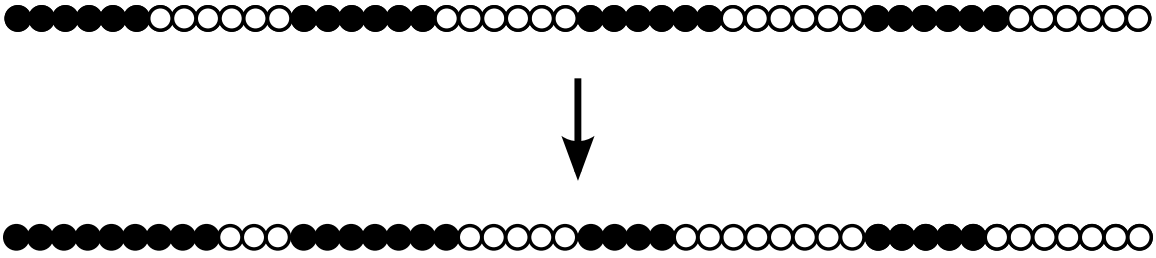

Figure 2.2: The regular diblock approximation is improved by approximating the chain as a series of equal-length diblocks with random compositions. In this image, $M = 4$.

$g_\alpha(n, s)$, which introduces the polydispersity; and the distribution $P(n)$, which gives the range of the polydispersity.

2.1 Segment Ensembles

In the present study, four different segment ensembles were used: homopolymers, diblocks, compositionally polydisperse symmetric triblocks, and sequentially polydisperse asymmetric triblocks. These ensembles are chosen, not because random copolymers are explicitly manufactured this way, but because it allows us to investigate separately the effects of different kinds of randomness. For example, the diblock and symmetric triblock models will have identical compositional variance, but different sequential arrangement. The asymmetric triblock model features sequential randomness exclusively, and has not compositional variance. The homopolymer model is equivalent to a simple random copolymer (equal pairing probabilities), and is the only ensemble in our model that can also be described by the Markovian models.

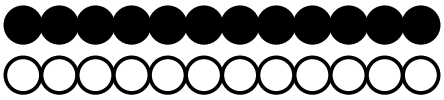

Figure 2.3: Homopolymer segments are equal-length A or B homopolymers.

2.1.1 Homopolymer Segments

The simplest ensemble is one in which each segment is assumed to be composed of either A or B. The probability of choosing one or the other is given by the total monomer fraction f_A. This also corresponds to the simplest type of random copolymer in the Markov-type models.

2.1.2 Diblock Copolymers

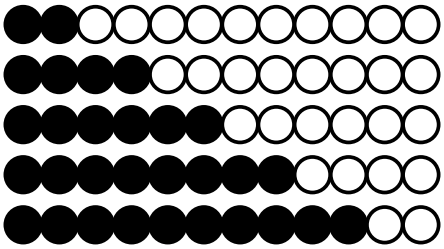

Figure 2.4: Model segments composed of compositionally polydisperse AB diblocks.

Each segment in this ensemble is an AB diblock copolymer. The total composition of each segment n is drawn from a distribution $P(n)$. $P(n)$ is chosen such that it is normalized and that $\langle n \rangle = f_A$:

$$\int_0^1 dn P(n) = 1, \tag{2.1}$$

$$\int_0^1 dn P(n) n = f_A. \tag{2.2}$$

2.1.3 Compositionally Polydisperse Symmetric Triblocks

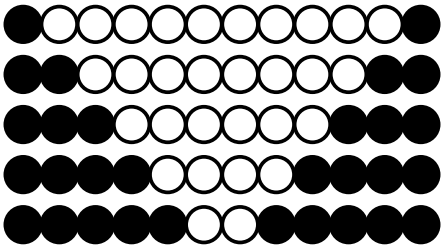

Figure 2.5: Model segments composed of compositionally polydisperse symmetric ABA triblocks.

Each segment is this ensemble is a symmetric ABA triblock copolymer. Again, the total composition of each segment n is drawn from a distribution $P(n)$. $P(n)$ is chosen such that it is normalized and that $\langle n \rangle = f_A$.

2.1.4 Sequentially Polydisperse Asymmetric Triblocks

The total composition of each segment in this ensemble is fixed. The position of the middle block is drawn from the distribution $P(n)$. $n = 0$ would correspond to the limiting case of an AB diblock while $n = 1$ would correspond to the limiting case of a BA diblock. $P(n)$ is chosen such that it is normalized and that $\langle n \rangle$ is equal to the average position of the middle block.

2.1.5 Modified Schulz Distribution

For the homopolymer segment ensemble, the distribution is a Bernoulli distribution with $P(0) = f_A$ and $P(1) = 1 - f_A$. For the remaining models, the distribution

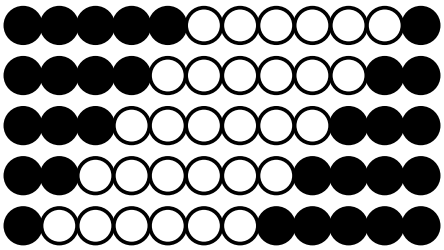

Figure 2.6: Model segments composed of compositionally monodisperse, asymmetric ABA triblocks.

function needs to be specified. When modelling a polydispersity system, the distribution of choice is often the Schulz distribution [9] which has the unnormalized form,

$$P(n) = n^{\alpha-1} e^{-\frac{\alpha n}{\langle n \rangle}}, \tag{2.3}$$

where n is a particular block length and α parametrizes the width of the distribution. α is related to the polydispersity index (PDI). The PDI is a typical measure of polydispersity and is defined as the ratio of the weight average molecular weight to the number average molecular weight,

$$\text{PDI} = \left(\frac{\sum\limits_i N_i M_i^2}{\sum\limits_i N_i M_i} \right) \left(\frac{\sum\limits_i N_i}{\sum\limits_i N_i M_i} \right), \tag{2.4}$$

where N_i is the number of polymers with molecular weight M_i. The system is perfectly monodisperse if PDI $= 1$. For the Schulz distribution, the PDI is related to the parameter α by,

$$\text{PDI} = \frac{\alpha + 1}{\alpha}. \tag{2.5}$$

For our model, we require that all the segments have the same length. If the segments are diblock copolymers, we require that the lengths of the A and B blocks

satisfy $n_A + n_B = 1$ (scaled to some reference length). Imagine an ensemble of polydisperse diblocks where each block is governed by the Schulz distribution (assuming the same α for both). If we filter the polymers so that they all have a particular length, the distribution for the filtered ensemble is given by the product of two Schulz distributions $P(f_A, n)$ and $P(1 - f_A, 1 - n)$,

$$P(n) = C\,(n(1-n))^{\alpha-1}\, e^{-\frac{\alpha n(1-2f_A)}{f_A(1-f_A)}}, \tag{2.6}$$

where C is a normalization constant. For our purposes, $f_A = \frac{1}{2}$ which lets us write this modified Schulz distribution as,

$$P(n) = C\,(n(1-n))^{\alpha-1}. \tag{2.7}$$

When α approaches 1, this distribution becomes a flat distribution. As α becomes large, it approaches a delta distribution. It will be convenient to define a new parameter,

$$\alpha = \frac{1}{1-\beta}, \tag{2.8}$$

so that the distribution function can be written as,

$$P(n) = C\,(n(1-n))^{\frac{\beta}{1-\beta}}. \tag{2.9}$$

One advantage of using β to parametrize the distribution is that it will make the range of numbers more manageable. $\beta = 1$ corresponds to a monodisperse distribution, while $\beta = 0$ corresponds to a flat distribution. This distribution over a range of β is

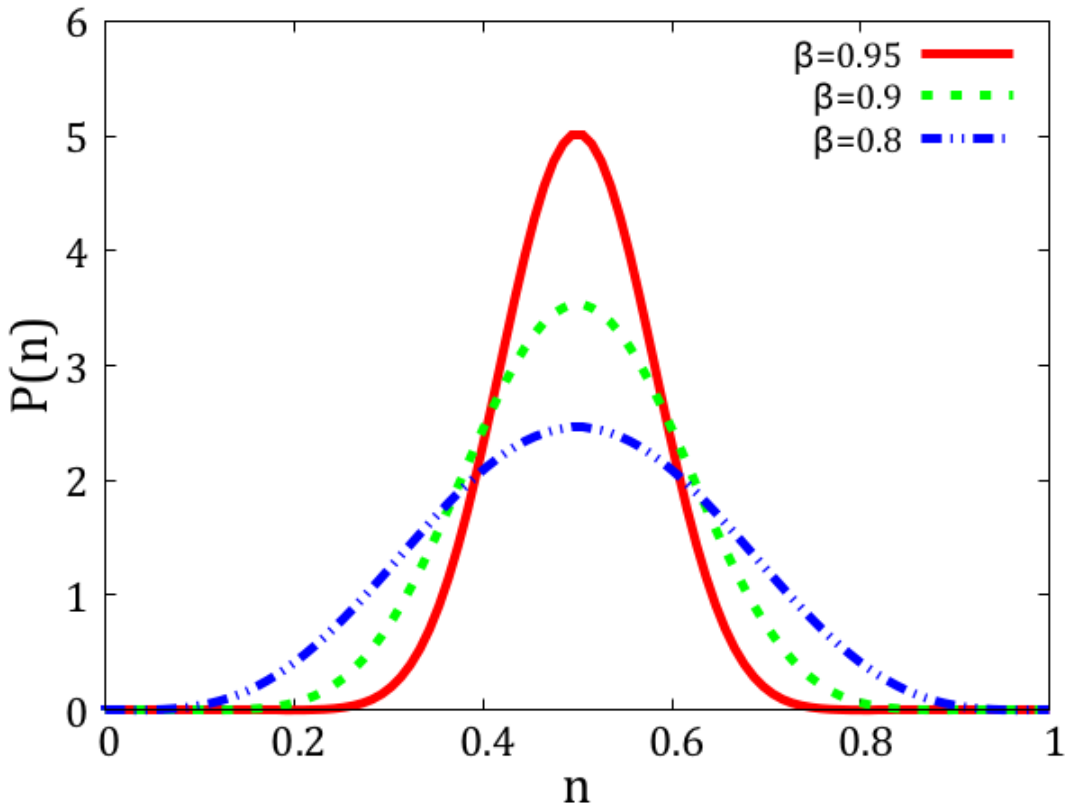

Figure 2.7: The modified Schulz distribution over a range of β.

shown in Figure 2.7. Although this distribution was derived for diblock segments, it will be used for all three continuous segment models so that they may be compared directly.

2.2 Implementation of the Segment Model into the Random Phase Approximation

Because evaluating the specific phase behaviour of a polydisperse block copolymer melt can be a formidable computational task, it is convenient to first have a general description of the phase behaviour. The random phase approximation (RPA) is a technique used to determine the stability of the disordered phase. It was first used by Leibler to calculate the spinodal of a diblock copolymer melt [10], but could be easily modified for any chain architecture. Briefly stated, the RPA uses a Landau expansion of the free energy in terms of the order parameter $\psi(q)$, which is the Fourier transform of the deviation of the local monomer concentration from the disordered state,

$$\psi(r) = \phi_A(r) - \bar{\phi}_A. \tag{2.10}$$

It can be shown that the 2nd order term in the expansion is proportional to the inverse of the structure factor $S(q)$ of the disordered state [10]. In the case of a monodisperse polymer melt composed of A and B monomers, the inverse structure factor is given by,

$$S^{-1}(q) = \frac{\sum_{\alpha,\beta} G_{\alpha\beta}(q)}{\det \mathbf{G}} - 2\chi_{AB}, \tag{2.11}$$

where $G_{\alpha\beta}(q)$ is the second-order single chain correlation function. $G_{\alpha\beta}(q)$ is given by the expression,

$$G_{\alpha\beta}(q) = N \int_0^1 ds \int_0^1 ds' g_\alpha(s) g_\beta(s') e^{-R_g^2 q^2 |s-s'|}, \tag{2.12}$$

where $g_\alpha(s)$ is the composition profile (the local concentration of α monomers at contour position s), N is the degree of polymerization, and R_g is the radius of gyration [11]. The radius of gyration will be taken as the unit length scale, which means we can set $R_g = 1$. Since N is a multiplicative factor common to all the correlation functions, we will factor it out of the expression for $G_{\alpha\beta}(q)$ and redefine the inverse structure factor as,

$$S^{-1}(q) = \frac{\sum_{\alpha,\beta} G_{\alpha\beta}(q)}{N \det \mathbf{G}} - 2\chi_{AB}, \tag{2.13}$$

Although the inverse structure factor is a function of q, each q corresponds to a particular fluctuation mode. The stability of the disordered state can be determined by checking the minimum value $S^{-1}(q)_{min}$. If $S^{-1}(q)_{min} < 0$, then local deviations from the homogenous state lower the free energy of the system. The spinodal line is determined by the condition $S^{-1}(q)_{min} = 0$. The critical value of χ_{AB} can be found by finding the q the minimizes $S^{-1}(q)$ (call it q') and rearranging,

$$\chi_{AB} N = \frac{\sum_{\alpha,\beta} G_{\alpha\beta}(q')}{2 \det \mathbf{G}(q')}. \tag{2.14}$$

In order to implement the Segment Model into the RPA the correlation functions must be replaced with their ensemble averages [12, 7],

$$G_{\alpha\beta}(q) \to \langle G_{\alpha\beta}(q) \rangle \,. \tag{2.15}$$

The averaged correlation function is an weighted integral over the entire sequence

space,

$$\langle G_{\alpha\beta}(q)\rangle = \int d\{n\}P(\{n\}) \int_0^1 ds \int_0^1 ds' g_\alpha(\{n\},s) g_\beta(\{n\},s') e^{-q^2|s-s'|}. \tag{2.16}$$

One of the two fundamental assumptions of the segment model is that the sequences of different segments are independent of one another. This allows the integral over the sequence space to be written explicitly as,

$$\langle G_{\alpha\beta}(q)\rangle = \left(\prod_{i=1}^{M} \int dn_i P(n_i)\right) \int_0^1 ds \int_0^1 ds' g_\alpha(\{n\},s) g_\beta(\{n\},s') e^{-q^2|s-s'|}. \tag{2.17}$$

The computational cost of this integral increases exponentially with the number of segments M. However, a significant simplification can be obtained by invoking the second fundamental assumption, that all the segments are of equal length. This allows the integrals over the contour to be divided into a sum of integrals over each segment,

$$\begin{aligned}\langle G_{\alpha\beta}(q)\rangle = \sum_{i=1}^{M}\sum_{j=1}^{M} \int dn_i P(n_i) \int dn_j P(n_j) \int_{\frac{i-1}{M}}^{\frac{i}{M}} ds \int_{\frac{j-1}{M}}^{\frac{j}{M}} ds' g_\alpha(n_i, Ms - i + 1) * \\ g_\beta(n_j, Ms' - j + 1) e^{-q^2|s-s'|}.\end{aligned} \tag{2.18}$$

Now consider separately the parts of the integral that correspond to a particular i

and j,

$$\langle G_{\alpha\beta}(q)\rangle_{ij} = \int dn_i P(n_i) \int dn_j P(n_j) \left[\int_{\frac{i-1}{M}}^{\frac{i}{M}} ds \int_{\frac{i-1}{M}}^{\frac{i}{M}} ds' g_\alpha(n_i, s) g_\beta(n_i, s') + \right.$$
$$\int_{\frac{i-1}{M}}^{\frac{i}{M}} ds \int_{\frac{j-1}{M}}^{\frac{j}{M}} ds' g_\alpha(n_i, s) g_\beta(n_j, s') + \int_{\frac{j-1}{M}}^{\frac{j}{M}} ds \int_{\frac{i-1}{M}}^{\frac{i}{M}} ds' g_\alpha(n_j, s) g_\beta(n_i, s') +$$
$$\left. \int_{\frac{j-1}{M}}^{\frac{j}{M}} ds \int_{\frac{j-1}{M}}^{\frac{j}{M}} ds' g_\alpha(n_j, s) g_\beta(n_j, s') \right] e^{-q^2|s-s'|}. \tag{2.19}$$

It can immediately be observed that the above expression divides neatly into 'intrablock' and 'interblock' components. We will proceed by first looking at the intrablock component,

$$\begin{aligned} \langle G_{\alpha\beta}(q)\rangle_{ij}^{(0)} &= \int_{\frac{i-1}{M}}^{\frac{i}{M}} ds \int_{\frac{i-1}{M}}^{\frac{i}{M}} ds' \left\langle g_\alpha(Ms - i + 1) g_\beta(Ms' - i + 1)\right\rangle e^{-q^2|s-s'|} + \\ &+ \int_{\frac{j-1}{M}}^{\frac{j}{M}} ds \int_{\frac{j-1}{M}}^{\frac{j}{M}} ds' \left\langle g_\alpha(Ms - j + 1) g_\beta(Ms' - j + 1)\right\rangle e^{-q^2|s-s'|} \\ &= \frac{2}{M^2} \int_0^1 ds \int_0^1 ds' \left\langle g_\alpha(s) g_\beta(s')\right\rangle e^{-q^2|s-s'|} \end{aligned} \tag{2.20}$$

Because this expression is independent of i and j, it is convenient to define *the* intrablock component as,

$$\langle G_{\alpha\beta}(q)\rangle^{(0)} = \frac{1}{M^2} \int_0^1 ds \int_0^1 ds' \left\langle g_\alpha(s) g_\beta(s')\right\rangle e^{-\frac{q^2|s-s'|}{M}}. \tag{2.21}$$

Because these functions appear frequently, the following short-hand will now be introduced,

$$\langle g_{\alpha\beta}(s,s')\rangle \equiv \langle g_\alpha(s) g_\beta(s')\rangle \,. \tag{2.22}$$

Moving on to the 'interblock' component,

$$\begin{aligned}\langle G_{\alpha\beta}(q)\rangle_{ij}^{(1)} = &\int_{\frac{i-1}{M}}^{\frac{i}{M}} ds \int_{\frac{j-1}{M}}^{\frac{j}{M}} ds' \,\langle g_\alpha(Ms-i+1)\rangle \,\langle g_\beta(Ms'-j+1)\rangle \, e^{-q^2|s-s'|} \\ &+ \int_{\frac{j-1}{M}}^{\frac{j}{M}} ds \int_{\frac{i-1}{M}}^{\frac{i}{M}} ds' \,\langle g_\alpha(Ms-j+1)\rangle \,\langle g_\beta(Ms'-i+1)\rangle \, e^{-q^2|s-s'|}. \end{aligned} \tag{2.23}$$

Adjusting the limits of integration,

$$\begin{aligned}\langle G_{\alpha\beta}(q)\rangle_{ij}^{(1)} = &\frac{1}{M^2}\int_0^1 ds \int_0^1 ds' \,\langle g_\alpha(s)\rangle \,\langle g_\beta(s')\rangle \, e^{-\frac{q^2|s-s'+i-j|}{M}} \\ &+ \frac{1}{M^2}\int_0^1 ds \int_0^1 ds' \,\langle g_\alpha(s)\rangle \,\langle g_\beta(s')\rangle \, e^{-\frac{q^2|s-s'-i+j|}{M}}. \end{aligned} \tag{2.24}$$

Let $m = |j-i|$ to remove any explicit dependency on i and j. Assuming that $j > i$,

$$\begin{aligned}\langle G_{\alpha\beta}(q)\rangle_m^{(1)} &= \frac{1}{M^2}\int_0^1 ds \int_0^1 ds' \,\langle g_\alpha(s)\rangle \,\langle g_\beta(s')\rangle \left(e^{-\frac{q^2|s-s'-m|}{M}} + e^{-\frac{q^2|s-s'+m|}{M}}\right) \\ &= \frac{1}{M^2}\int_0^1 ds \int_0^1 ds' \,\langle g_\alpha(s)\rangle \,\langle g_\beta(s')\rangle \left(e^{\frac{q^2(s-s'-m)}{M}} + e^{-\frac{q^2(s-s'+m)}{M}}\right) \\ &= \frac{e^{-\frac{q^2 m}{M}}}{M^2}\int_0^1 ds \int_0^1 ds' \,\langle g_\alpha(s)\rangle \,\langle g_\beta(s')\rangle \, 2\cosh\left(\frac{q^2(s-s')}{M}\right). \end{aligned} \tag{2.25}$$

Because the hyperbolic cosine is symmetric about the origin, this result does not depend on the condition $j > i$. The assumption was made only to show explicitly how to get rid of the absolute value brackets in the exponential functions. It is seen that the interblock component of this subsection of the correlation function does not depend explicitly on i and j, but only on the degree of separation between the segments, m. As before, it will be convenient to define *the* interblock component,

$$\langle G_{\alpha\beta}(q)\rangle^{(1)} = \frac{1}{M^2}\int_0^1 ds \int_0^1 ds' \,\langle g_\alpha(s)\rangle \,\langle g_\beta(s')\rangle \, 2\cosh\left(\frac{q^2(s-s')}{M}\right), \tag{2.26}$$

which gives the specific interblock component with degree of separation m to be,

$$\langle G_{\alpha\beta}(q)\rangle^{(m)} = e^{-\frac{q^2 m}{M}} \langle G_{\alpha\beta}(q)\rangle^{(1)}, m > 0. \tag{2.27}$$

A further simplification can be made by a change of variables $\tilde{q} = \frac{q}{\sqrt{M}}$, which will remove any explicit dependency on M from $\langle G_{\alpha\beta}(q)\rangle^{(0)}$ and $\langle G_{\alpha\beta}(q)\rangle^{(1)}$. Furthermore, there is a common multiplicative factor of $\frac{1}{M^2}$ which can be factored out leading to more general expressions for the intrablock and interblock correlation functions,

$$\langle G_{\alpha\beta}(\tilde{q})\rangle^{(0)} = \int_0^1 ds \int_0^1 ds' \,\langle g_{\alpha\beta}(s,s')\rangle \, e^{-\tilde{q}^2|s-s'|}, \tag{2.28}$$

$$\langle G_{\alpha\beta}(\tilde{q})\rangle^{(1)} = \int_0^1 ds \int_0^1 ds' \,\langle g_\alpha(s)\rangle \,\langle g_\beta(s')\rangle \, 2\cosh\left(\tilde{q}^2(s-s')\right), \tag{2.29}$$

with the inverse structure factor redefined as,

$$S^{-1}(\tilde{q}) = \frac{M^2}{N}\frac{\sum_{\alpha\beta}\langle G_{\alpha\beta}(\tilde{q})\rangle}{\det\langle \mathbf{G}\rangle} - 2\chi_{AB}. \tag{2.30}$$

The complete correlation functions used in equation (2.30) are found by simply adding up the different components according to the number of times that each degree of separation m occurs:

$$\begin{aligned}\langle G_{\alpha\beta}(\tilde{q})\rangle &= M\langle G_{\alpha\beta}(\tilde{q})\rangle^{(0)} + \sum_{i=1}^{M-2}\sum_{j=i+1}^{M-1} e^{-\tilde{q}^2|i-j|}\langle G_{\alpha\beta}(\tilde{q})\rangle^{(1)} \\ &= M\langle G_{\alpha\beta}(\tilde{q})\rangle^{(0)} + \sum_{m=1}^{M-1}(M-m)e^{-\tilde{q}^2 m}\langle G_{\alpha\beta}(\tilde{q})\rangle^{(1)}\end{aligned} \tag{2.31}$$

The benefit of this result is that the $(M+2)$-dimensional integral of equation (2.16) can always be expressed as a sum of two 2-dimensional integrals, making the computational cost of the RPA calculations actually *independent* of the complexity of the chain M.

Assuming a two-component system, the statistical properties of the random copolymers are specified by defining five functions: the two average composition functions $\langle g_A(s)\rangle$ and $\langle g_B(s)\rangle$; and the three coupled average composition functions $\langle g_{AA}(s,s')\rangle$, $\langle g_{BB}(s,s')\rangle$, $\langle g_{AB}(s,s')\rangle$:

$$\langle g_\alpha(s)\rangle = \int dn P(n) g_\alpha(n,s), \tag{2.32}$$

$$\langle g_{\alpha\beta}(s,s')\rangle = \int dn P(n) g_\alpha(n,s) g_\beta(n,s'). \tag{2.33}$$

Note that locally, $\langle g_{\alpha\beta}(s,s')\rangle \neq \langle g_{\beta\alpha}(s,s')\rangle$. However, these functions only appear

in integrals with an $s \leftrightarrow s'$ exchange symmetry which means that, at least for our purposes, $\langle g_{AB}(s,s')\rangle$ and $\langle g_{BA}(s,s')\rangle$ can be used interchangeably. Depending on the segment model used, these functions could be difficult to calculate. Using the constraint $g_A(s) = 1 - g_B(s)$, it can be shown that these functions are related as follows:

$$\langle g_B(s)\rangle = 1 - \langle g_A(s)\rangle\,, \tag{2.34}$$

$$\langle g_{BB}(s,s')\rangle = 1 - \langle g_A(s)\rangle - \langle g_A(s')\rangle + \langle g_{AA}(s,s')\rangle\,, \tag{2.35}$$

$$\langle g_{AB}(s,s')\rangle = \langle g_A(s)\rangle - \langle g_{AA}(s,s')\rangle\,. \tag{2.36}$$

Thus, only $\langle g_A(s)\rangle$ and $\langle g_{AA}(s,s')\rangle$ need to be calculated to obtain the entire set of composition functions.

Equation (2.31) can be used for any random copolymer melt that satisfies that two restrictions of the model, namely equal length segments and statistical independence of the individual segment sequences, and where all the segments are drawn from the same distribution. This last requirement is not a fundamental requirement of the model. In the next section, the RPA implementation will be generalized to allow for more complicated chain architectures involving multiple segment distributions.

2.2.1 RPA Implementation with Multiple Segment Ensembles

The model as previously implemented assumed that each segment in the chain is drawn from the same ensemble. A useful extension of the model, which will greatly increase its flexibility, is to allow for multiple ensembles of segments. For example, some segments can be specifically chosen to be diblocks, and some can be specifically chosen to be triblocks. Additionally, this allows for more complex arrangements of different chemical components, such as an A/B random copolymer linked to a C homopolymer, as will be shown in this section. As before, the integral breaks up into intrablock and interblock components. The intrablock component is the same as before,

$$\langle G_{\alpha\beta}(\tilde{q})\rangle_X^{(0)} = \int_0^1 ds \int_0^1 ds' \, \langle g_{\alpha\beta}(s,s')\rangle_X \, e^{-\tilde{q}^2|s-s'|}. \tag{2.37}$$

Note that an additional subscript is required in order to specify the type of segment. Turning to the interblock component, it must now be specified what the order of the segments is. For example, an AB diblock followed by a BA diblock will have a different interblock component than a BA diblock followed by an AB diblock.

Let the i^{th} segment be drawn from distribution X and the j^{th} segment be drawn

from distribution Y. If $j > i$ and $m = |j - i|$, then,

$$\begin{aligned}
\langle G_{\alpha\beta}(\tilde{q})\rangle_{XY}^{(m)} &= \int_0^1 ds \int_0^1 ds' \, \langle g_\alpha(s)\rangle_X \, \langle g_\beta(s')\rangle_Y \, e^{-\tilde{q}^2|s-s'+i-j|} \\
&+ \int_0^1 ds \int_0^1 ds' \, \langle g_\alpha(s)\rangle_Y \, \langle g_\beta(s')\rangle_X \, e^{-\tilde{q}^2|s-s'+j-i|}. \\
&= \int_0^1 ds \int_0^1 ds' \, \langle g_\alpha(s)\rangle_X \, \langle g_\beta(s')\rangle_Y \, e^{-\tilde{q}^2|s-s'-m|} \\
&+ \int_0^1 ds \int_0^1 ds' \, \langle g_\alpha(s)\rangle_Y \, \langle g_\beta(s')\rangle_X \, e^{-\tilde{q}^2|s-s'+m|}. \\
&= e^{-\tilde{q}^2 m} \int_0^1 ds \int_0^1 ds' \Big(\langle g_\alpha(s)\rangle_X \, \langle g_\beta(s')\rangle_Y \, e^{\tilde{q}^2(s-s')} \\
&+ \langle g_\alpha(s)\rangle_Y \, \langle g_\beta(s')\rangle_X \, e^{-\tilde{q}^2(s-s')} \Big) \\
&= e^{-\tilde{q}^2 m} \int_0^1 ds \int_0^1 ds' \, \big(\langle g_\alpha(s)\rangle_X \, \langle g_\beta(s')\rangle_Y \\
&+ \langle g_\beta(s)\rangle_X \, \langle g_\alpha(s')\rangle_Y \big) \, e^{\tilde{q}^2(s-s')}.
\end{aligned} \tag{2.38}$$

When all the segments are identical, symmetry shows that the results are the same, whether $(i > j)$ or $(j > i)$. Except for the particular case where the average profiles are themselves symmetric about their centre, it must always be specified whether X is downstream or upstream from Y. In my notation, $\langle G_{\alpha\beta}(\tilde{q})\rangle_{XY}^{(1)}$ indicates that

the X block preceeds the Y block. There is no general prefactor for the interblock components, but must be found specifically for the system of interest.

As an example, I will now write the second-order single-chain correlation function for a melt of polymers in which each chain consists of a random copolymer of type X with $M/2$ segments covalently bonded at one end to a random copolymer of type Y with $M/2$ segments. I will assume that the orientation of the segments is such that X segments are upstream from the Y segments.

To begin, we can first calculate the two intrablock correlation functions,

$$\langle G_{\alpha\beta}(\tilde{q})\rangle_X^{(0)} = \int_0^1 ds \int_0^1 ds' \, \langle g_{\alpha\beta}(s,s')\rangle_X \, e^{-q^2|s-s'|}, \tag{2.39}$$

and,

$$\langle G_{\alpha\beta}(\tilde{q})\rangle_Y^{(0)} = \int_0^1 ds \int_0^1 ds' \, \langle g_{\alpha\beta}(s,s')\rangle_Y \, e^{-q^2|s-s'|}. \tag{2.40}$$

It will be necessary to define three interblock correlation functions,

$$\langle G_{\alpha\beta}(\tilde{q})\rangle_{XX}^{(1)} = \int_0^1 ds \int_0^1 ds' \, \langle g_\alpha(s)\rangle_X \, \langle g_\beta(s')\rangle_X \, 2\cosh\left(\tilde{q}^2(s-s')\right), \tag{2.41}$$

$$\langle G_{\alpha\beta}(\tilde{q})\rangle_{YY}^{(1)} = \int_0^1 ds \int_0^1 ds' \, \langle g_\alpha(s)\rangle_Y \, \langle g_\beta(s')\rangle_Y \, 2\cosh\left(\tilde{q}^2(s-s')\right), \tag{2.42}$$

$$\begin{aligned}\langle G_{\alpha\beta}(\tilde{q})\rangle_{XY}^{(1)} = \int_0^1 ds \int_0^1 ds' \, \big(&\langle g_\alpha(s)\rangle_X \, \langle g_\beta(s')\rangle_Y + \\ &\langle g_\beta(s)\rangle_X \, \langle g_\alpha(s')\rangle_Y\big) \, e^{\tilde{q}^2(s-s')}.\end{aligned} \tag{2.43}$$

It is not necessary to define $\langle G_{\alpha\beta}(\tilde{q})\rangle^{(1)}_{YX}$ because all of the X segments are assumed to be upstream from the Y segments. As before, the complete correlation function is found by summing up the different interblock and intrablock components with the appropriate prefactors,

$$\langle G_{\alpha\beta}(\tilde{q})\rangle = \frac{M}{2}\langle G_{\alpha\beta}(\tilde{q})\rangle^{(0)}_{X} + \frac{M}{2}\langle G_{\alpha\beta}(\tilde{q})\rangle^{(0)}_{Y} + \left(\sum_{m=1}^{M/2-1}(M/2-m)e^{-\tilde{q}^2 m}\right)\langle G_{\alpha\beta}(\tilde{q})\rangle^{(1)}_{XX} + \left(\sum_{m=1}^{M/2-1}(M/2-m)e^{-\tilde{q}^2 m}\right)\langle G_{\alpha\beta}(\tilde{q})\rangle^{(1)}_{YY} + \left(\sum_{m=1}^{M-1}(M-|m-M|)e^{-\tilde{q}^2 m}\right)\langle G_{\alpha\beta}(\tilde{q})\rangle^{(1)}_{XY}. \tag{2.44}$$

Although there are more functions to be calculated, the computational cost remains independent of M.

2.2.2 Macrophase Separation

Previous studies have predicted that under certain conditions random copolymers could undergo macroscopic phase separation [3, 4, 5]. For example, simple random copolymers do not microphase separate, but only undergo macrophase separation at the ODT. For a melt of random copolymers, it may be difficult to imagine what macrophase separation looks like in that situation. In a melt of A and B homopolymers, the polymers macrophase separate into A and B domains which are mostly composed of just A or B homopolymers. In a melt of random copolymers, some chains are A-rich and some chains are B-rich. In macrophase separation, the A-rich polymers separate from the B-rich polymers leading to disordered A-rich and B-rich domains whose local composition depends on the compositional variance of the entire melt. This situation is more complicated than the homopolymer because the chains exist on a continuum of compositions instead of just being all A or all B. As such, both macrophase and microphase separation are possible. The RPA can be used to derive some interesting characteristics of macrophase separation (should it occur). In the RPA, macrophase separation is obtained if the minimum of $S^{-1}(q)$ occurs at $q = 0$. Physically, this corresponds the absence of a finite length scale in the ordered state of the system.

Assuming that $q = 0$ minimizes the inverse structure factor, the average correlation function is simply given by,

$$\langle G_{\alpha\beta} \rangle = \left\langle \int_0^1 \int_0^1 ds ds' g_\alpha(s) g_\beta(s') \right\rangle = \langle f_\alpha f_\beta \rangle \,. \tag{2.45}$$

Substituting this into the expression for the inverse structure factor, we get,

$$S^{-1} = \frac{1}{N}\frac{\langle f_A f_A\rangle + 2\langle f_A f_B\rangle + \langle f_B f_B\rangle}{\langle f_A f_A\rangle\langle f_B f_B\rangle - \langle f_A f_B\rangle^2} - 2\chi_{AB}. \tag{2.46}$$

We are looking for the critical point, so we need χ_{AB} such that $S^{-1} = 0$:

$$\chi_{AB}N = \frac{\langle f_A f_A\rangle + 2\langle f_A f_B\rangle + \langle f_B f_B\rangle}{2\langle f_A f_A\rangle\langle f_B f_B\rangle - 2\langle f_A f_B\rangle^2} = \frac{1}{2\mathrm{var}(f_A)}. \tag{2.47}$$

It will be useful to write this expression in terms of the variance of a single segment:

$$\mathrm{var}(f_A)_{\mathrm{chain}} = \left\langle \left(\sum_{i=1}^{M}\frac{f_{A_i}}{M}\right)^2\right\rangle - \left\langle \sum_{i=1}^{M}\frac{f_{A_i}}{M}\right\rangle^2 = \frac{\mathrm{var}(f_A)_{\mathrm{segment}}}{M}. \tag{2.48}$$

Therefore, in the regime of macrophase separation, the critical point is given by the number of segments divided by twice the variance of a single segment,

$$\chi_{AB}N = \frac{M}{2\mathrm{var}(f_A)_{\mathrm{segment}}}. \tag{2.49}$$

2.3 Implementation of the Segment Model into Self-Consistent Field Theory

In order to evaluate the full phase behaviour of the random copolymer melt, it will be necessary to implement the segment model into self-consistent field theory (SCFT). SCFT is mean-field theory that reduces the many-particle polymer melt to a single chain in a field. The free energy of the system is minimized using a saddle-point approximation, which leads to a set of mean-field equations. Each solution to the mean-field equations is a potential equilibrium phase for the system. The relative stability of the different candidate structures is found by comparing their free energy densities. The structure with the lowest free energy is the stable phase. The computational challenge is in finding the solutions of the mean-field equations. This is often done by starting with an approximation of a candidate structure, and using an iteration scheme to continually adjust the fields until they satisfy the equations to some tolerance. The length scales need to be adjusted as well, so that the free energy is minimized with respect to the period of the structure. Depending on the size of the box, and the complexity of the structure, finding a solution to the mean-field equations can range from minutes to days. A more detailed explanation of the self-consistent mean field theory can be found in several reviews from the literature [13, 14, 15, 16, 17, 18, 19].

For a monodisperse melt, where each polymer has an identical sequence profile

$g_\alpha(s)$, the self-consistent field theory equations are,

$$\phi_\alpha(\mathbf{r}) = \frac{1}{Q}\int_0^1 ds g_\alpha(s) q(\mathbf{r},s) q^\dagger(\mathbf{r},s), \tag{2.50}$$

$$\omega_\alpha(\mathbf{r}) = \sum_{\beta\neq\alpha} \chi_{\alpha\beta} N \phi_\beta(\mathbf{r}) + \eta(\mathbf{r}), \tag{2.51}$$

$$\sum_\alpha \phi_\alpha(\mathbf{r}) = 1, \tag{2.52}$$

where $\phi_\alpha(\mathbf{r})$ is the local concentration of α-type monomers; Q is the single-chain partition function;$q(\mathbf{r},s)$ and $q^\dagger(\mathbf{r},s)$ are the end-integrated propagators; $\omega_\alpha(\mathbf{r})$ is the potential field; $\chi_{\alpha\beta}$ are the Flory-Huggins parameters; N is the degree of polymerization; and $\eta(\mathbf{r})$ is a Lagrange multiplier to ensure incompressibility. The propagators satisfy the modified diffusion equations (MDE),

$$\frac{\partial}{\partial s} q(\mathbf{r},s) = \frac{b^2 N}{6}\nabla^2 q(\mathbf{r},s) - \left(\sum_\alpha \omega_\alpha(\mathbf{r},s) g_\alpha(s)\right) q(\mathbf{r},s), \tag{2.53}$$

$$-\frac{\partial}{\partial s} q^\dagger(\mathbf{r},s) = \frac{b^2 N}{6}\nabla^2 q^\dagger(\mathbf{r},s) - \left(\sum_\alpha \omega_\alpha(\mathbf{r},s) g_\alpha(s)\right) q^\dagger(\mathbf{r},s), \tag{2.54}$$

with initial conditions $q(\mathbf{r},0) = 1$ and $q^\dagger(\mathbf{r},1) = 1$. V is the volume of the box. b is the Kuhn length, which is related to the radius of gyration by $R_g = b\sqrt{\frac{N}{6}}$. R_g is the length scale used in these calculations which allows the pre-factor of $\frac{b^2 N}{6}$ to be dropped from the diffusion term of the MDE. The partition function Q can be obtained through,

$$Q = \frac{1}{V}\int d\mathbf{r} q^\dagger(\mathbf{r},0) \tag{2.55}$$

For our purposes, we are dealing not with a monodisperse melt with a single profile

$g_\alpha(s)$, but with a polydisperse melt with a distribution of profiles $g_\alpha(\{n\}, s)$. This means that the weighted contribution to the total monomer concentration from each individual sequence needs to be taken into account,

$$\begin{aligned}\phi_\alpha(\mathbf{r}) &= \left\langle \frac{1}{Q_{\{n\}}} \int_0^1 ds g_\alpha(\{n\}, s) q_{\{n\}}(\mathbf{r}, s) q^\dagger_{\{n\}}(\mathbf{r}, s) \right\rangle \\ &= \left(\prod_{i=1}^{M} \int dn_i P(n_i) \right) \frac{1}{Q_{\{n\}}} \int_0^1 ds g_\alpha(\{n\}, s) q_{\{n\}}(\mathbf{r}, s) q^\dagger_{\{n\}}(\mathbf{r}, s). \end{aligned} \tag{2.56}$$

In order to proceed, it will be necessary to integrate the partition function over the sequence space. A brute force method would be to approximate each integral as a sum,

$$\int dn P(n) F(n) \approx \sum_{j=1}^{S} P_j F(n_j), \tag{2.57}$$

where F(n) is the function being integrated and S is the number of terms in the sum. How this approximation is set up can be optimized on a case-by-case basis, depending on the distribution, but the general method used in this thesis is a equal-spaced summation with,

$$n_j = \int_{(j-1)/S}^{j/S} dn P(n) n, \tag{2.58}$$

and,

$$P_j = \int_{(j-1)/S}^{j/S} dn P(n) \tag{2.59}$$

The problem with such an approach is that it requires solving S^M MDE's per iteration, which means that the (already considerable) computational cost increases exponentially with the dimensionality of the sequence space. For small M (e.g. 1, 2

or 3) it may be possible to do the integral in full; but for most cases it is necessary to resort to further approximations, two of which will be outlined next.

2.3.1 Single-Chain Approximation

The easiest approximation, as alluded to in section 2.1.1, is to ignore the sequence space integral entirely and assume a monodisperse melt. There are two ways of doing this: 1) set each segment parameter to the average value $n_i = \langle n \rangle$, or 2) pick a random set of M parameters $\{n\}$ using the distribution $P(n)$ and proceed as though this profile is common to all the chains. The benefit of these approaches is that they are computationally the most efficient.

The first version has the advantage of there being no asymmetry in how the sequence space is approximated. Calculations done by this method demonstrate the basic effects of blockiness on the phase behaviour, while assuming that the effects of randomness are minimal. This is the approach taken in this thesis, when the single-chain approximation is used.

The second method may show the effects of irregularity within the monomer sequence, but has the disadvantage of asymmetrically representing the sequence space, which may lead to artificial phase behaviour. For example, in the real system if one segment is unusually A-rich, there will be another chain whose corresponding segment is unusually B-rich. The overall disadvantage of the single-chain approximation is that inter-chain effects due to compositional variance are entirely ignored. It will be seen that these effects can be important to the type of phase behaviour displayed. For example, sufficiently high compositional variance can induce macrophase separation, something a single-chain approximation could not possibly describe.

2.3.2 Multi-Chain Approximation

In the full sequence space integral, the entire sequence space is written as a weighted sum, where the weight is determined by the probability distribution. If, for example, a single dimension of the sequence space is divided into 10 points, the MDE would have to be solved 1000 times per iteration in order to do the calculation with $M = 3$. An alternative would be to randomly sample the sequence space to create a smaller ensemble of chains. This subset will be taken as a complete representation of the larger melt, reducing the sequence space from a continuous, multidimensional space to a discrete set of chains. As such, the integral is no longer approximated as a weighted sum, but is simply,

$$\phi_\alpha(\mathbf{r}) = \sum_{i=1}^{S} \frac{1}{Q_{\{n\}_i}} \int_0^1 ds g_\alpha(\{n\}_i, s) q_{\{n\}_i}(\mathbf{r}, s) q^\dagger_{\{n\}_i}(\mathbf{r}, s), \tag{2.60}$$

where $\{n\}_i$ is the i^{th} set of parameters and S is the number of chains approximating the melt. The advantage of this method is that compositional variance effects are no longer ignored and that (ideally) S is large enough to assume that the sequence space has been sufficiently sampled. There is a much larger computational cost compared to the single-chain approximation. However, it is a good alternative in the case of large compositional variance, when the accuracy of the single-chain approximation is questionable. When the multi-chain approximation is used in this thesis, $S = 100$.

Chapter 3

Numerical Methods of SCFT

3.1 Pseudo-Spectral Method

The modified diffusion equation was first solved using a spectral algorithm introduced by Matsen and Schick in 1994 which scales as M^3, where M is the number of basis functions [20]. In 2002, Rasmussen and Kalosakas introduced a pseudo-spectral method for solving the modified diffusion equation which scales as $M \log M$ [21]. However, direct comparisons of efficiency are not so straightforward due to the fact that the spectral method can readily incorporate the symmetries of the morphology of interest in order to reduce the number of basis functions M [22]. In addition, the iteration method can significantly effect the rate of convergence. One immediate advantage of the pseudo-spectral method is that it is a real-space algorithm which makes it naturally suitable for more 'exploratory' calculations in which the dimensions and symmetries of the mesophase are not known *a priori*. The calculations done in this thesis use the 2nd-order Rasmussen-Kalosakas method (RK2), though 4th-order methods have also been developed by Ranjan, Qin, and Morse (RQM4) [23] as well as

by Cochran, Garcia-Cervera, and Fredrickson (CGF4) [24]. The algorithm is based on a symmetric split-step Fourier algorithm, more detailed explanations of which can be found in the literature (e.g [25]).

We will restrict ourselves to a one-dimensional form of the modified diffusion equation,

$$\frac{\partial}{\partial s}q(x,s) = \frac{\partial^2}{\partial x^2}q(x,s) - \omega(x)q(x,s), \tag{3.1}$$

where $q(x,s)$ is the end-integrated propagator, $\omega(x)$ is the mean-field, x is the real-space position, and s is the contour position. This can be recast as a first order differential equation by defining the linear operator $\mathcal{L}$,

$$\mathcal{L} \equiv \frac{\partial^2}{\partial x^2} - \omega(x). \tag{3.2}$$

This differential equation has a solution,

$$q(x,s) = e^{\mathcal{L}s}q(x,0). \tag{3.3}$$

Given a particular contour position $q(x,s)$, we can move a small step Δs along the chain to $s + \Delta s$,

$$q(x, s+\Delta s) = e^{\mathcal{L}\Delta s}q(x,s). \tag{3.4}$$

In order to implement the the exponential of the linear operator numerically, we can make an approximation by dividing it into three separate operators,

$$q(x, s+\Delta s) \approx e^{-\omega(x)\Delta s/2}e^{(\partial^2/\partial x^2)}e^{-\omega(x)\Delta s/2}q(x,s). \tag{3.5}$$

Note that these operators do not commute. If they did, this would not be an approximation but an exact solution. On a computer, these operators are represented by finite sized matrices, while the propagator is represented by a vector $q(s)_i$. We can rewrite the operators as,

$$D_{jk} = \left(e^{(\partial^2/\partial x^2)\Delta s}\right)_{jk}, \tag{3.6}$$

$$W_{jk} = \left(e^{-\omega(x)\Delta s/2}\right)_{jk}, \tag{3.7}$$

which gives,

$$q(s+\Delta s)_j \approx W_{jk} D_{kl} W_{lm} q(s)_m, \tag{3.8}$$

where a summation over the indices is implied. The mean-field matrix W is diagonal in real space though the diffusion matrix D is not diagonal in real-space. However, the diffusion matrix *is* diagonal in Fourier space. This follows from the fact that the Fourier space basis functions are eigenfunctions of the operator $\partial^2/\partial x^2$. Using $F^\dagger_{kj}$ and F_{kj} to represent the discrete Fourier transform and Inverse Fourier transform matrices, a single 'step' along the propagator can be represented by the matrix product,

$$\begin{aligned} q(s+\Delta s)_i &= W_{ik} F_{kl} F^\dagger_{lm} D_{mn} F_{no} F^\dagger_{op} W_{pq} q(s)_q \\ &= W_{ik} F_{kl} \hat{D}_{lm} F^\dagger_{mn} W_{no} q(s)_o \end{aligned} \tag{3.9}$$

The forward-reverse Fourier transform pairs can be inserted into the matrix product because of the property $F_{ij}F^\dagger_{jk} = \delta_{ik}$. The mean-field matrix, being diagonal in real-space, is simply given by,

$$W_{ij} = e^{-\omega(iL/n)\Delta s/2}\delta_{ij} \tag{3.10}$$

It can be shown that the diffusion matrix in Fourier space has elements,

$$\hat{D}_{ij} = \exp\left(-4\sin^2\left(\frac{\pi i}{n}\right)\Delta s\frac{n^2}{L^2}\right)\delta_{ij}, \tag{3.11}$$

where n the size of the matrix and L is the real-space size of the box (typically given in units of the radius of gyration R_g). Assuming n to be large, we can Taylor expand the argument of the exponential to write the matrix elements in the simpler form,

$$\hat{D}_{ij} = e^{-(2\pi i/nL)^2\Delta s}\delta_{ij}. \tag{3.12}$$

However, in this method, the proper reciprocal space basis to use is symmetric about the origin (the first Brillouin zone), leading to the more correct form of the reciprocal space representation of the diffusion matrix,

$$\hat{D}_{ij} = e^{-(2\pi i/nL)^2\Delta s}\delta_{ij}, \tag{3.13}$$

for $i = 0, 1, ..., M/2$ and

$$\hat{D}_{ij} = e^{-(2\pi (n-i)/nL)^2\Delta s}\delta_{ij}, \tag{3.14}$$

for $i = M/2 + 1, n/2 + 2, ..., M - 1$.

In summary, the method is as follows:

1. multiply the propator vector $q(s)_j$ by the mean-field matrix W_{ij} in real space.

$$q'(s)_i = W_{ij}q(s)_j$$

2. Fourier transform the result.

$$\hat{q}'(s)_i = F^{\dagger}_{ij} q'(s)_j$$

3. multiply the propagator by the diffusion matrix $\hat{D}_{ij}$ in reciprocal space.

$$\hat{q}''(s)_i = \hat{D}_{ij} \hat{q}'(s)_j$$

4. inverse Fourier transform the result.

$$q''(s)_i = F_{ij} \hat{q}''(s)_j \tag{3.15}$$

5. multiply the propator again by the mean-field matrix W_{ij} in real space.

$$q(s + \Delta s)_i = W_{ij} q''(s)_j$$

Note that because each matrix is diagonal in the space in which it is being multiplied, each vector-matrix multiplication requires only n operations instead of n^2 operations.

3.2 Anderson Mixing

Anderson mixing is an algorithm that can be used to find solutions iteratively to the SCFT equations more efficiently than by simple mixing. In the context of block copolymer SCFT, Anderson mixing is a 'least-squares' optimization method in which each successive guess in the iteration procedure is a linear combination of previous guesses. The Anderson mixing algorithm supplies the coefficients of the linear combination that minimizes the error, assuming a linear system. The pseudo-spectral implementations of Anderson mixing from Thompson and Matsen was used for all the SCFT results presented here [26, 27]. The procedure will be briefly stated here:

Given a 'guess' for the k^{th} iteration $\omega_\alpha^{(k)}(\mathbf{r})$, the new fields $\tilde{\omega}_\alpha^{(k)}(\mathbf{r})$ can be evaluated by solving the modified diffusion equation with $\omega_\alpha^{(k)}(\mathbf{r})$ and calculating the concentration fields $\phi_\alpha^{(k)}(\mathbf{r})$ and the incompressibility field $\eta^{(k)}(\mathbf{r})$. The deviation can be defined as the difference between $\omega^{(k)}$ and $\tilde{\omega}^{(k)}$,

$$d_\alpha^{(k)}(\mathbf{r}) = \tilde{\omega}_\alpha^{(k)}(\mathbf{r}) - \omega_\alpha^{(k)}(\mathbf{r}). \tag{3.16}$$

We can define an inner product,

$$(f(\mathbf{r}), g(\mathbf{r})) = \int d\mathbf{r} f(\mathbf{r}) g(\mathbf{r}), \tag{3.17}$$

from which we can define the total error,

$$\text{error} \equiv \left[\frac{\sum_\alpha (d_\alpha^{(k)}, d_\alpha^{(k)})}{\sum_\alpha (\omega_\alpha^{(k)}, \omega_\alpha^{(k)})} \right]^{1/2}, \tag{3.18}$$

which will be used to gauge the numerical inaccuracy of the solution during the calculation. The next set of input fields $\omega_\alpha^{(k+1)}(\mathbf{r})$ can be found by evaluating the matrix,

$$U_{ij} = \sum_\alpha \left(d_\alpha^{(k)} - d_\alpha^{(k-i)}, d_\alpha^{(k)} - d_\alpha^{(k-j)} \right), \tag{3.19}$$

and the vector,

$$V_i = \sum_\alpha \left(d_\alpha^{(k)} - d_\alpha^{(k-i)}, d_\alpha^{(k)} \right) \tag{3.20}$$

where the indices i and j from from 1 to H. H is the number of field histories used in the calculation. A vector of coefficients C_i is found through the product,

$$C_i = U_{ij}^{-1} V_j, \tag{3.21}$$

which as used to recombine the previous fields as,

$$W_\alpha^{(k)}(\mathbf{r}) = \omega_\alpha^{(k)}(\mathbf{r}) + \sum_{i=1}^{H} C_i \left(\omega_\alpha^{(k-i)}(\mathbf{r}) - \omega_\alpha^{(k)}(\mathbf{r}) \right), \tag{3.22}$$

and,

$$D_\alpha^{(k)}(\mathbf{r}) = d_\alpha^{(k)}(\mathbf{r}) + \sum_{i=1}^{H} C_i \left(d_\alpha^{(k-i)}(\mathbf{r}) - d_\alpha^{(k)}(\mathbf{r}) \right). \tag{3.23}$$

The new fields are given by,

$$\omega_\alpha^{(k+1)} = W_\alpha^{(k)} + \lambda D_\alpha^{(k)}, \tag{3.24}$$

where $0 < \lambda \leq 1$ is a mixing parameter.

There is a trade-off with the choice of λ. Larger values of λ tend to accelerate the convergence, though it can make the calculation unstable. Different approaches

have been used by various authors in their treatment of λ. Thompson, for example, uses simple mixing until the error is below a certain threshold, after which Anderson mixing is switched on with λ. This is also the approach used by Jiang et al. in their SCFT study of ABC star copolymers [28]. By contrast, Matsen uses Anderson mixing from the start, but gradually increases λ using,

$$\lambda = 1 - 0.9^k. \tag{3.25}$$

In my calculations, I have found that Anderson mixing has a tendency to get trapped in a metastable state. When this happens, the error plateaus at a value that is too large for the fields to properly be considered solutions to the SCFT field equations. One remedy that can alleviate this issue is to use Anderson mixing from the start and gradually increase λ using 3.25. After 25 iterations, I 'reset' the calculation by erasing the old histories and setting the iteration count to $k = 0$. The cost of this approach is that λ is never allowed to grow much, which slows down the process. However, it was found to significantly improve both the plateauing issue, as well as the stability of the calculation.

In simple mixing, the incompressibility field $\eta(\mathbf{r})$ can be found by incrementally adjusting the it after each iteration until it converges,

$$\eta^{(k+1)}(\mathbf{r}) = \eta^{(k)}(\mathbf{r}) - \gamma \left(1 - \sum_{\alpha} \phi_{\alpha}(\mathbf{r}) \right), \tag{3.26}$$

where $\gamma > 0$ is some mixing parameter. This method introduces great instability to the calculation when used with Anderson mixing, showing that an exact expression

for $\eta(\mathbf{r})$ is necessary. In the case of a two-component system, the field is simply,

$$\eta(\mathbf{r}) = \frac{1}{2}\left(\omega_A(\mathbf{r}) + \omega_B(\mathbf{r})\right) \tag{3.27}$$

In the work presented here, three-component systems were also examined, in which case $\eta(\mathbf{r})$ is given by,

$$\eta(\mathbf{r}) = \frac{\sum_\alpha \omega_\alpha(\mathbf{r}) X_\alpha - 2N\chi_{AB}\chi_{BC}\chi_{AC}}{\sum_\alpha X_\alpha}, \tag{3.28}$$

where $X_A = \chi_{BC}(\chi_{AB} + \chi_{AC} - \chi_{BC})$, $X_B = \chi_{AC}(\chi_{AB} + \chi_{BC} - \chi_{AC})$, and $X_C = \chi_{AB}(\chi_{AC} + \chi_{BC} - \chi_{AB})$ [28, 21].

The procedure runs until the error is below a given threshold. Matsen suggests 10^{-5}. For my convergence threshold, I let the code run until the error is less than 10^{-4} and the change in free energy between iterations is less than 10^{-7}. This is because the free energy was often found to converge faster than the fields, and that the difference in free energies between candidate structures was at least on the order of 10^{-3}, but was typically on the order of 10^{-2}, making this degree of convergence more than sufficient.

Chapter 4

$A/B - C \rightarrow ABC$ Pseudo-Phase Transition

A particularly interesting random copolymer architecture is a random copolymer composed of A and B monomers covalently bonded at one end to a homopolymer of C monomers (Figure 4.1). This class of polymer will be notated as $A/B - C$. Assuming that the A, B, and C monomers are immiscible, there are three general categories of phase behaviour that one may observe. The first is a purely homogeneous disordered phase. The second is an ordered phase with distinct A, B, and C domains (hereafter referred to as ABC phase behaviour). The third is an ordered phase with a distinct C domain and a homogeneous A/B domain (hereafter referred to as $A/B-C$ phase behaviour). This third form of phase behaviour can occur when the enthalpic interactions are strong enough to phase separate the random A/B blocks from the C blocks, but not strong enough to overcome the entropic barrier to phase separation within the A/B block itself. As the interaction parameter χ_{AB} is increased, eventually the A/B blocks will be able to phase separate, leading to ABC phase behaviour.

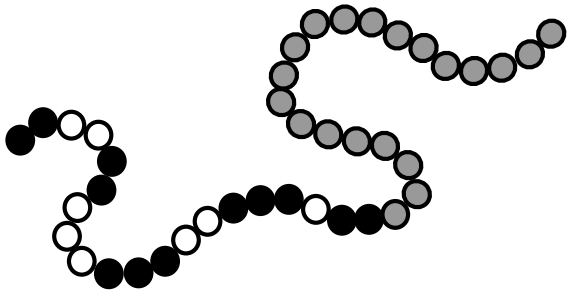

Figure 4.1: Schematic of an $A/B-C$ random copolymer

The transition from $A/B-C$ to ABC phase behaviour is not a true phase transition. Rather, it is just a gradual change in the morphology of the ordered state. As such, there is an inherent ambiguity as to whether a given structure is most properly labelled $A/B-C$ or ABC. For example, lamellar profiles of the chain architecture $(ABA)_4C$ with different values of χ_{AB} are shown in Figure 4.2. What is observed is a gradual transition from a simple lamellar profile to a hierarchical lamellar profile. The top and bottom profiles are clearly of type $A/B-C$ and ABC respectively, while intermediate case (shown in the middle) is less clear. It should be noted that the ambiguity is not in whether or not there is a deviation from the pure $A/B-C$ state, but whether or not the morphology distinct A and B domains. For example, in Figure 4.2 (middle panel), there are two clear peaks in the B profile, but the concentration is such that there is not local excess of B monomers.

This problem has been addressed previously by Weihua Li and An-Chang Shi in a study on hierarchical lamellar structures from $A(BC)_nBA$ multiblock copolymers [29]. In this particular system, the B and C blocks form hierarchical lamellar structures between two A layers. In order to differentiate between $B/C-A$ and ABC

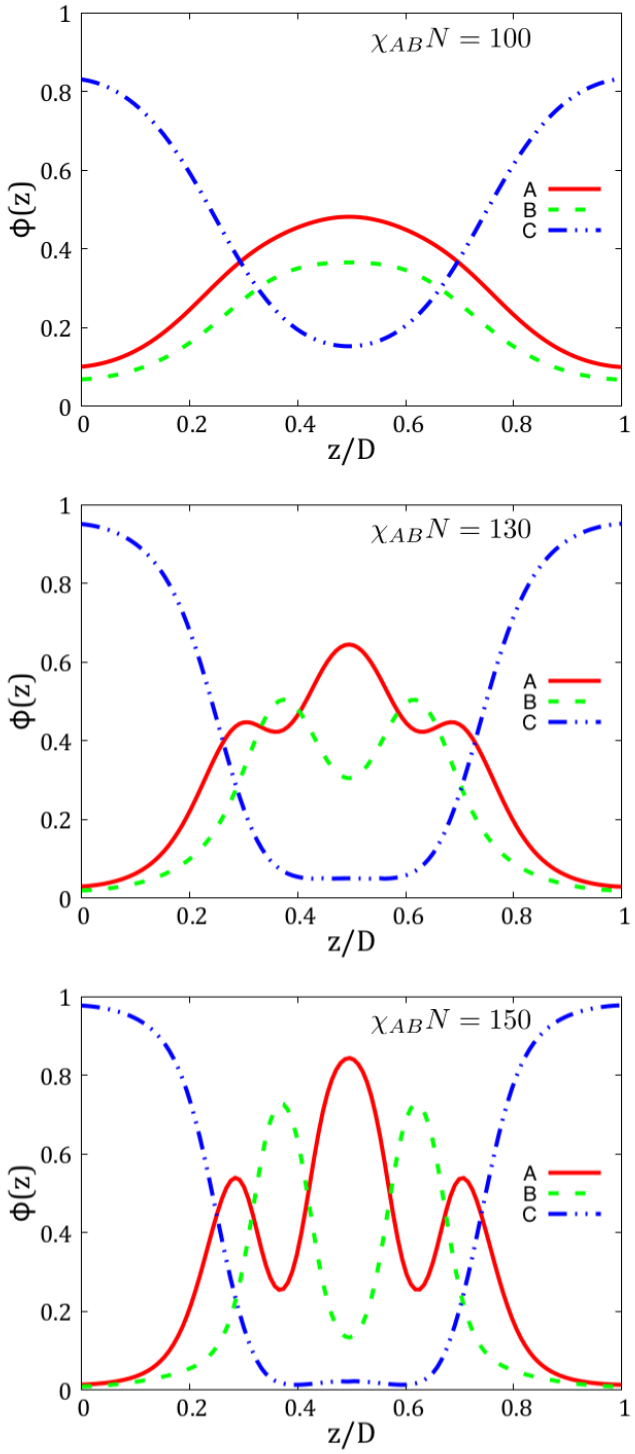

Figure 4.2: Density profiles for the lamellar structure at various $\chi_{AB}N$. From top to bottom, the profiles correspond to $\chi_{AB}N = 100, 130, 150$. The period of the lamellar structure is D.

domain ordering, a new order parameter $\Delta\phi_C$ was defined,

$$\Delta\phi_C = \frac{1}{\bar{\phi}_C}\frac{1}{x_2 - x_1}\int_{x_1}^{x_2} |\phi_C(x) - \bar{\phi}_C(x)|dx, \tag{4.1}$$

where $\bar{\phi}_C = \frac{1}{x_2 - x_1}\int_{x_1}^{x_2}\phi_C(x)$ is the average density of C monomers within the region x_1 to x_2. The region is chosen to be in the centre of the hierarchical lamellar structure so as to be minimally influenced by the $B/C - A$ interface. The phase is considered to be a simple lamellar until $\Delta\phi_C$ crosses chosen threshold, typically on the order of $\Delta\phi_C = 0.05$.

In this thesis, a slightly different approach is taken. I define an order parameter ψ as an integral over the entire domain,

$$\psi = \int dz|f_A\phi_B(z) - f_B\phi_A(z)|. \tag{4.2}$$

This is an integral of the local concentration deviations of the random A/B block from a perfect $A/B - C$ phase. In the purely 'disordered' A/B state, $\psi = 0$ and grows monotonically as the random block phase separates. As in [29], it would possible to choose a threshold for ψ above which the system is said to be in the ABC regime. Alternatively, we can first look at the the order parameter as a function of χ_{AB} (Figure 4.3). The curve has a sigmoid-like shape, with an inflection point around $\chi = 135$ and $\psi = 0.03$. This inflection point ($\frac{d^2\psi}{d\chi^2} = 0$) provides a clear definition for the $A/B - C \rightarrow ABC$ transition that is intrinsic to the system itself.

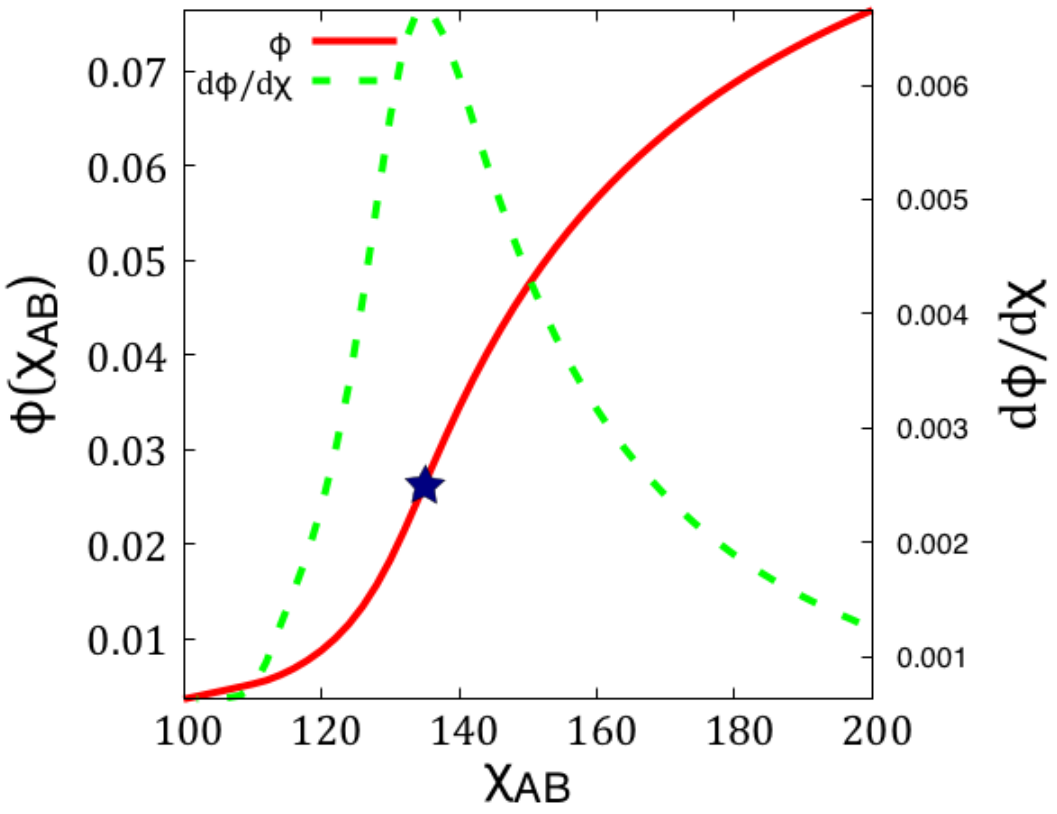

Figure 4.3: Example of the order parameter ψ as a function of χ_{AB}. Plotted with it is the derivative $d\psi/d\chi$. The curve has a clear inflection point at about $\chi = 135$ (marked with a star).

Chapter 5

Candidate Structures

Candidate structures used in the SCFT calculations are drawn from the usual four diblock structures: body centred cubic (BCC) (Figure 5.1), gyroid (Figure 5.2), hexagonally packed cylinders (HPC) (Figure 5.3), and lamellar. Several different hierarchical lamellar morphologies were found to be stable for the $A/B-C$ random copolymers (Figure 5.4). These structures consist of alternating layers of A and B domains sandwiched between two C domains. The ordering of these domains is always $C(ABA)_nC$, owing to the particular architecture and Flory-Huggins parameters used in these calculations. The different lamellar structures are labelled lam_n where n is the number of distinct B layers in one period. lam_d refers to the 'disordered' lamellar structure, consisting of distinct C domains and blended A/B domains (as was explained in more detail in chapter 4). The equivalent hierarchical HPC structures were examined as well but were never found to be stable.

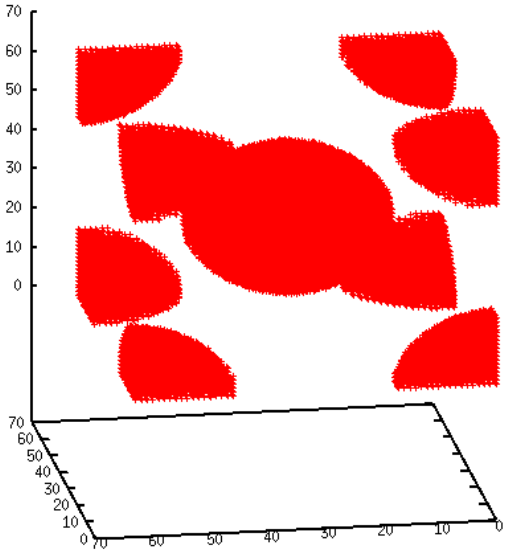

Figure 5.1: Example of the body centered cubic structure.

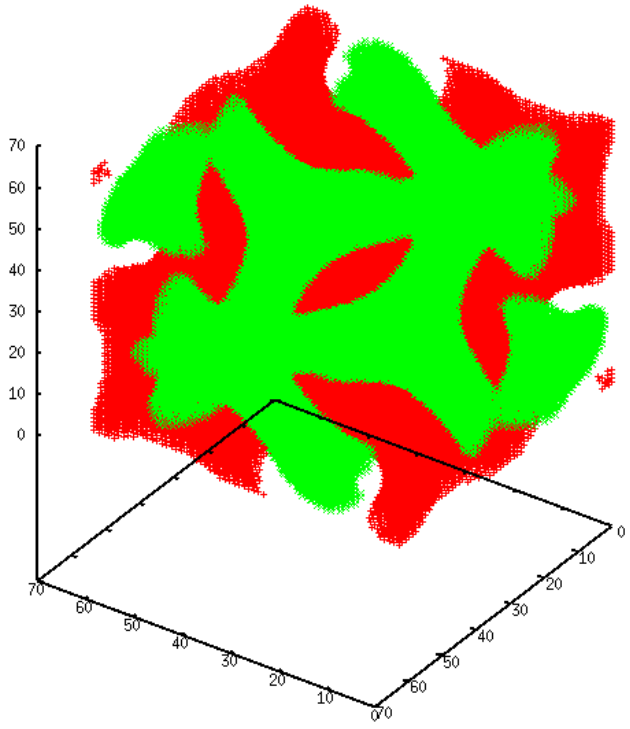

Figure 5.2: Example of the gyroid structure.

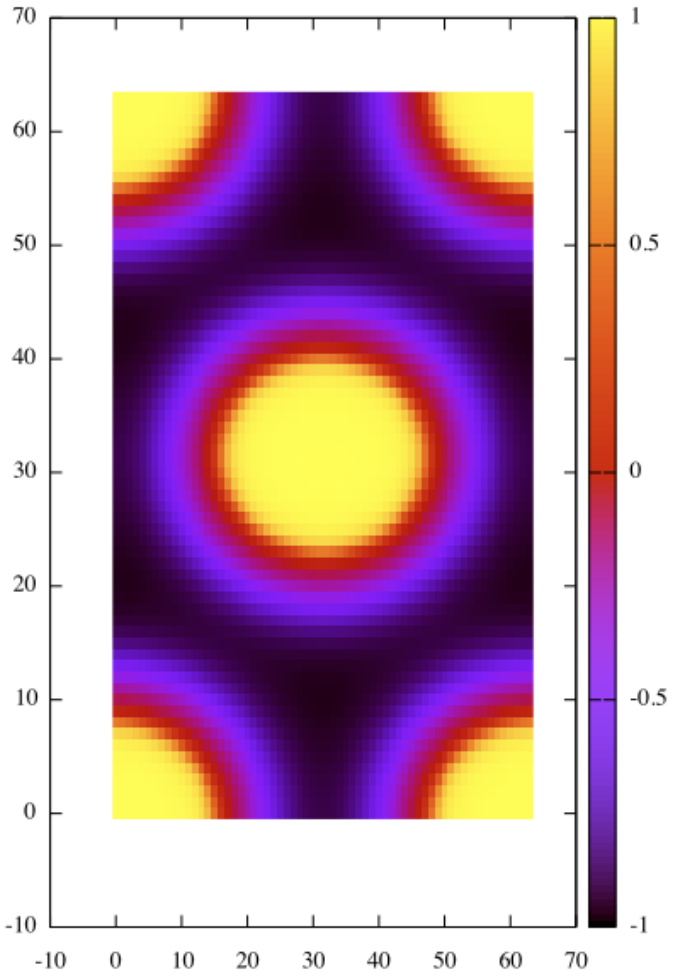

Figure 5.3: Example of the hexagonally packed cylinder structure.

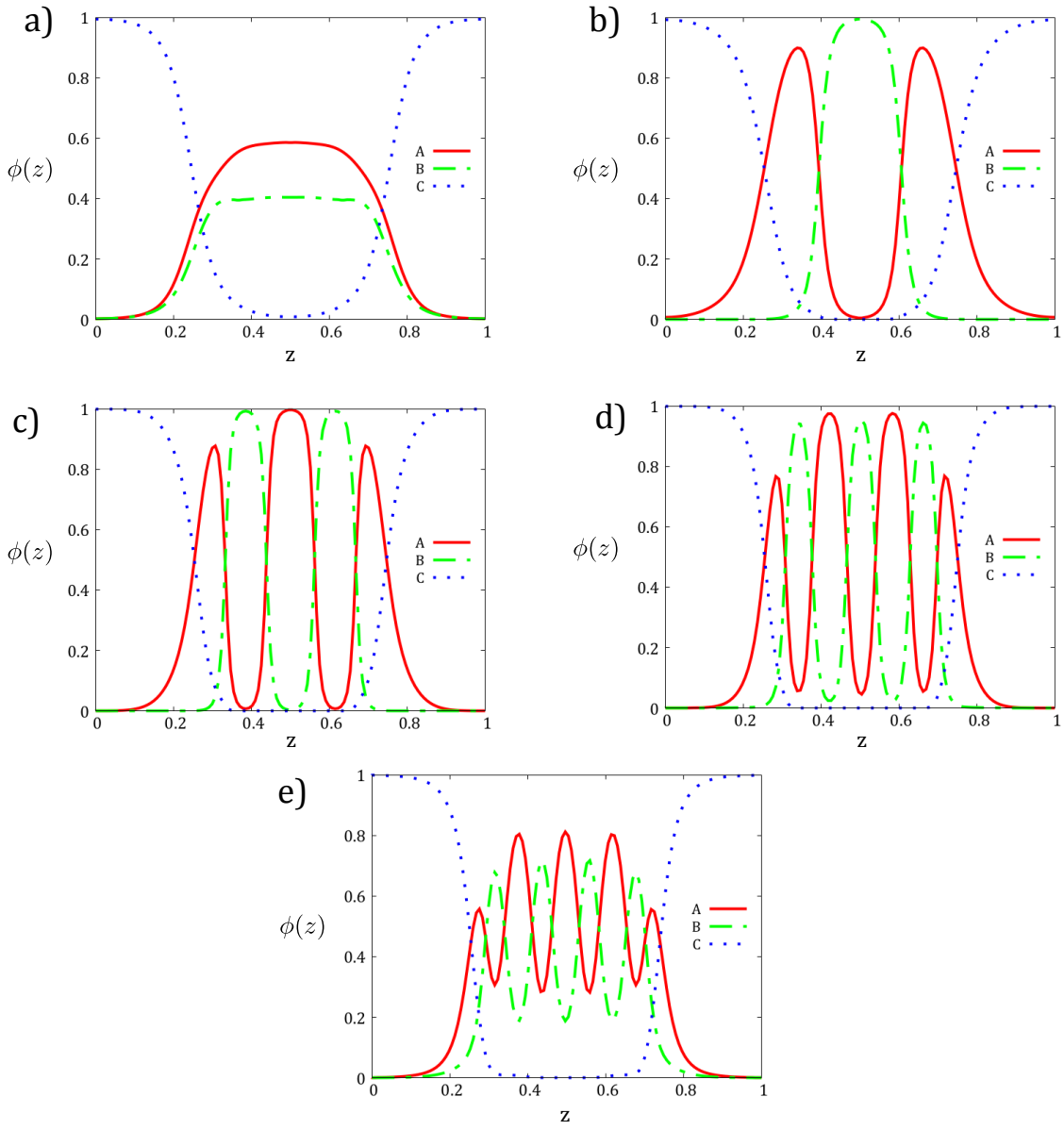

Figure 5.4: Profiles of the hierachical lamellar structures: a) lam_d, b) lam_1, c) lam_2, d) lam_3, e) lam_4.

Chapter 6

Results and Discussion

6.1 Effects of Blockiness and Polydispersity on the Order-Disorder Transtion of Random Block Copolymers

The first set of calculations performed were done with the aim of investigating the effects of randomness on the order-disorder transition (ODT) of various types of random copolymer melts. The RPA implementation of the segment model was used to calculate the critical point as a function of M and distribution width β for the four segment ensembles previously outlined: homopolymers, diblock copolymers, symmetric triblock copolymers, and asymmetric triblock copolymers.

6.1.1 Homopolymer Segment Ensemble

Although the critical point must be calculated numerically in general, for the case of homopolymer segments, it can be obtained analytically. This choice of segments corresponds to a simple random copolymer with equal 'like' and 'unlike' monomer pairings. As such, it is the only random copolymer in our model that also appears in the Markovian random copolymer models. We first need to calculate the average composition profiles:

$$\langle g_A(s) \rangle = f_A(1) + (1 - f_A)(0) = f_A, \tag{6.1}$$

$$\langle g_{AA}(s, s') \rangle = f_A(1)(1) + (1 - f_A)(0)(0) = f_A. \tag{6.2}$$

Substituting these into the expression for the inverse structure factor gives,

$$S(q)^{-1} = \frac{1}{N} \frac{M}{f_A(1 - f_A) \int_0^1 ds \int_0^1 ds' e^{-q^2|s-s'|}} - 2\chi. \tag{6.3}$$

This function has a minimum at $q = 0$, implying a macrophase separation. Setting $S^{-1}(0) = 0$ and solving for χ gives the critical point of the system to be,

$$\chi N = \frac{M}{2f_A(1 - f_A)}, \tag{6.4}$$

which is the same expression derived for the simple random copolymer [3].

6.1.2 Dependence of the Critical Point on Blockiness

For any given choice of segments, the blockiness is parametrized by the number of segments used in each chain, M. The blockiness, was previously defined as $b = \frac{1}{M}$. The degree of polymerization N is assumed to be fixed. Therefore increasing M does not lengthen the chain, but further subdivides it. For the homopolymer segment ensemble, it was shown in the previous section that the critical value of χ_{AB} is proportional to M, or inversely proportional to the blockiness. Similarly, it was shown that in the case of macrophase separation that the critical point is always proportional to M, regardless of the choice of segments. For more complicated segment ensembles, the critical point will have to be calculated numerically. This was done for the three remaining segment ensembles: diblocks, symmetric triblocks, and asymmetric triblocks, according to the method derived in section 2.2. Plotting the critical points with various distribution widths β as a function of M (Figure 6.5) it is generally observed that the critical points approach a linear proportionality to M ($\chi_c N \sim M$). This linear relation does not appear to be dependent on the distribution width. The slope of the critical value of χN as a function of M decreases with a broadening distribution, showing that increasing the randomness lowers the critical point. Qualitatively, the trends from the diblock and symmetric triblock ensembles are similar, particularly when M is big. Interestingly, the asymmetric triblock, while showing the same trend, appears much diminished in its effect. Noting that the asymmetric triblock ensemble is compositionally monodisperse, it would appear that the effects of sequential and compositional dispersity could be strikingly different in magnitude.

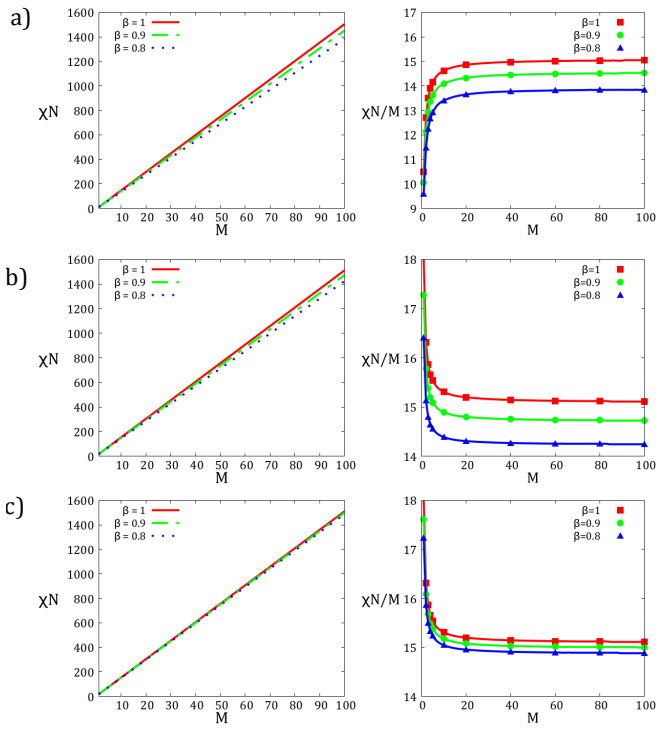

Figure 6.5: The order-disorder point of the diblock segment ensemble plotted over a range of blockiness M and distribution width β. a) AB diblock segment ensemble, b) ABA symmetric triblock ensemble, c) ABA asymmetric triblock ensemble

6.1.3 Dependence of the Phase Behaviour on Distribution Width

Fixing M, the critical points for the different (continuous) segment ensembles can be plotted as a function of β. Starting with $M = 1$, for particularly blocky chains, we immediately observe several interesting features (Figure 6.6). In the limit of a monodisperse melt ($\beta = 1$), the two triblock ensembles coincide (as they should) though they quickly diverge as randomness is introduced. Around $\beta = 0.7$, there is a 'kink' in the symmetric triblock critical point followed by a change in concavity. Approaching $\beta = 0$ (a flat distribution) the diblock and symmetric triblock ensembles converge. Examining the wave vector q that minimizes the inverse structure factor, we see a discontinuity and the β that corresponds to the kink. At this point, q jumps from a finite value to 0. This shows that the system is actually switching at this point from microphase separation to macrophase separation, which makes the kink a Lifshitz point [30].

Repeating this with $M = 100$, we observe several interesting differences (Figure 6.6). Firstly, in the limit of a monodisperse melt, all three segment ensembles roughly coincide. This makes sense since apart from the endpoints, the diblock and triblock chains are essentially identical. Now, as the randomness increases, both the symmetric triblock and diblock ensembles exhibit a Lifshitz point. When they are both in regimes of macrophase separation, their critical points converge. This is explained by the fact that both of these ensembles have the same compositional variance. It was previously shown that in the case of macrophase separation, the critical point is determined entirely by the compositional variance. Since both the diblock and symmetric triblock ensembles have compositions drawn from the same distribution, they have the

same compositional variance. The asymmetric triblock ensemble never macrophase separates. This is due to the fact that this ensemble has zero compositional variance, and hence cannot be divided into A-rich and B-rich domains.

As was previously stated, because these chains exist on a continuum of compositions and sequences, it is not clear whether macrophase or microphase separation will be observed. For example, in the case $M = 1$ why does the balance tip in favour of macrophase separation for the symmetric triblock ensemble yet not for the diblock ensemble, even though compositionally the two ensembles are the same? Presumably the answer lies in the higher entropic barrier to microphase separation found in an ABA triblock copolymer compared with the compositionally identical AB diblock copolymer [31, 32]. Sequential and compositional dispersity are seen to have different effects on phase behaviour, both in terms of phenomenon and magnitude. A simple illustration for this difference can be obtained by considering how these two kinds of reordering 'demix' the monomer components of the melt. The most mixed state possible would be a melt of identical polymers whose local monomer concentration is $g_A(s) = f_A$. There are two ways to demix the monomers: by exchanging monomers within the chains or by exchanging monomers between the chains (Figure 6.7).

Demixing by exchanging monomers within the chains will create A-rich and B-rich regions within the chains. Within a mesophase, the configurational freedom of the chains is limited by the $A-B$ junctions, which are confined to the $A-B$ interfaces of the structure. If the blocks are short, there is less configurational freedom available to the chains between the junctions than if they were long. If the block lengths are increased, which can be done by intra-chain exchange, the entropic barrier to microphase separation can be reduced due to the newly available configurational

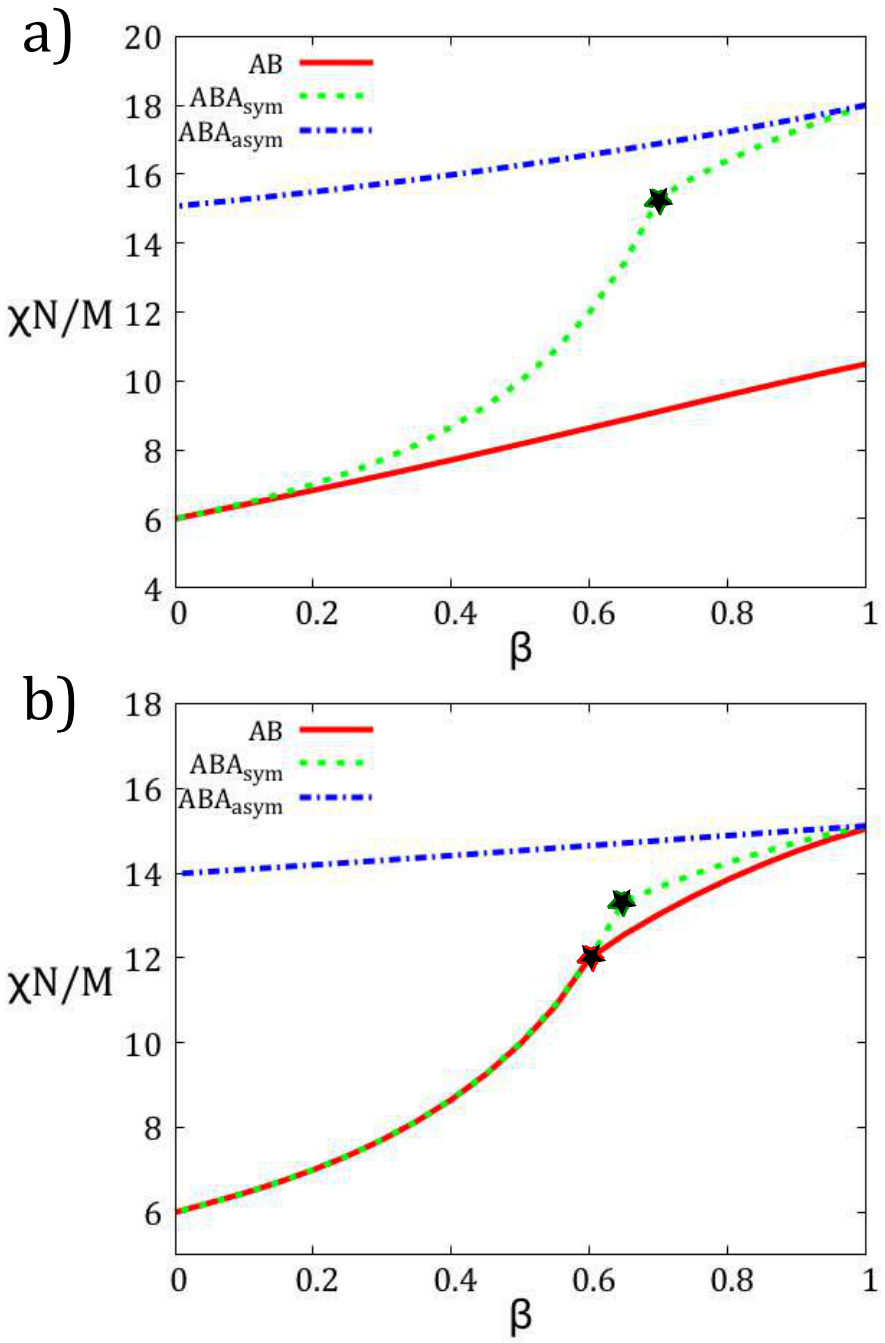

Figure 6.6: The order-disorder critical point of the continuous segment ensembles plotted as a function of β with M fixed. The Lifshitz point is indicated with a star. a) M=1, b) M=100

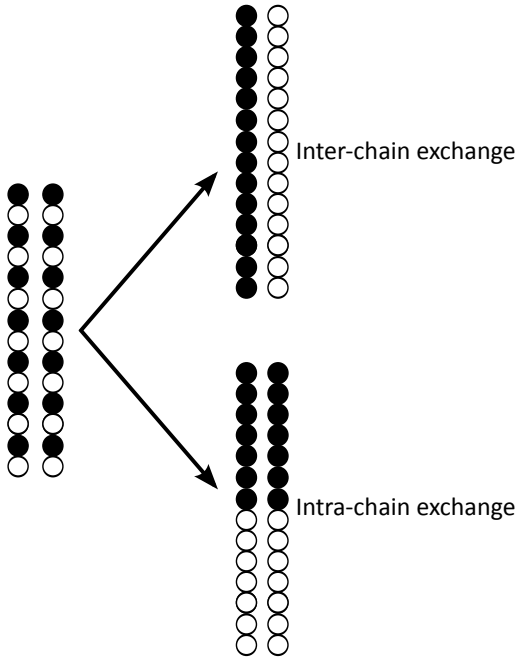

Figure 6.7: Unmixing the monomers by exchanging within or between chains can lead to different phase behaviour.

freedom. On the other hand, demixing by inter-chain exchange will not only create A-rich and B-rich regions within the chains, but will increase the compositional variance of the system. In macrophase separation, the system is divided into large disordered A-rich and B-rich domains (microphase separation can later occur if χ is increased further). The enthalpy of these domains is less than the unseparated homogeneous state. However, there is a large cost in entropy when the system is divided like this. The reduction in enthalpy increases with the compositional variance. However, because the A-rich and B-rich domains are also created within chains, the barrier to microphase separation is also reduced, just as in intra-chain exchange. There is, therefore, a competition between the reduction in free energy due to microphase separation, and the reduction due to macrophase separation. This competition can

be directly observed in Figure 6.6. For the symmetric triblock ensemble with $M = 1$, and for the diblock and symmetric triblock ensembles with $M = 100$, microphase separation is preferred only when the compositional variance is low. Eventually, the compositional variance is large enough that the scale tips in favour of macrophase separation. It could be argued that much of the effect arises not just within the chains but between them. For example, consider the diblock ensemble with $M = 1$. A monodisperse melt made from any individual sequence in this ensemble would have a higher critical value than that of the symmetric diblock. Yet, when combined together the critical value is lower than that of the symmetric diblock. The critical point of these random copolymer melts was always seen to be less than $\chi N = 10.5$, which is the critical point of a melt of symmetric diblocks. This question has been studied in the theory of Markov-type random copolymers and the theoretical study of the phase behaviour has gone beyond the ODT into specific predictions on the ordered phases including the transitions from disordered macrophase separated domains to ordered macrophase separated domains [33].

6.1.4 Comparison with Self-Consistent Field Theory

For the sake of comparison, the critical point as a function of β was calculated using SCFT for the case $M = 1$. Because this is just a one-dimensional sequence space, the integral was solved in full, using equation 2.31 with $S = 9$. The calculation was done for each of the continuous segment ensembles previously discussed. The lamellar structures were found for a χN near the predicted ODT and was incrementally reduced until the ordered structure could no longer be maintained. At each value

of χN, the free energy was minimized with respect to the box size. These threshold values of χN give an approximate location of the critical point. There excellent agreement between the RPA and SCFT calculations as per the location of the critical point. Additionally, for the symmetric triblock ensemble, the domain spacing of the lamellar structure calculated by SCFT was seen to diverge between $\beta = 0.7$ and $\beta = 0.6$. This indicates a transition to macrophase separation in perfect agreement to that predicted by the RPA calculations (Figure.6.8).

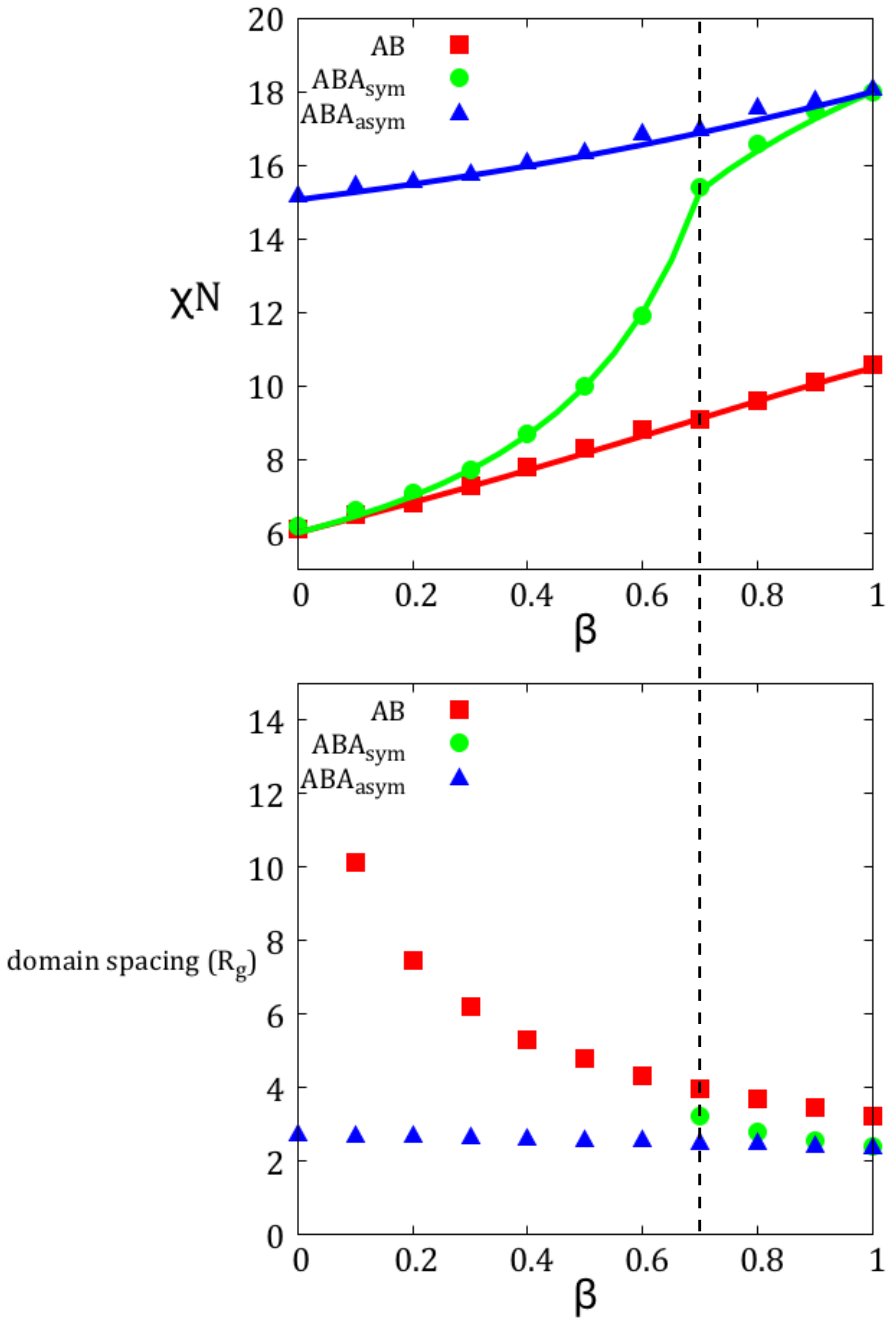

Figure 6.8: above: Comparision of the predicted critical point by RPA (lines) with the approximated critical point by SCFT (points). below: the domain spacing of the lamellar structure as a function of distribution width β. The Lifshitz point is indicated by a dotted line. Note that for the ABA_{sym} ensemble, there is no defined domain size past the Lifshitz point

6.2 Phase Behaviour of $A/B-A$ Random Copolymers

In this section, the phase behaviour of $A/B-A$ random copolymers will be investigated using the RPA and SCFT. In particular, the system is a random copolymer with a 50/50 fraction of A and B monomers joined at one end to a homopolymer of type A. Within the segment model, the random chain is treated as a series of M, ABA triblocks, while the homopolymer is treated as a series of M, A blocks (Figure 6.9).

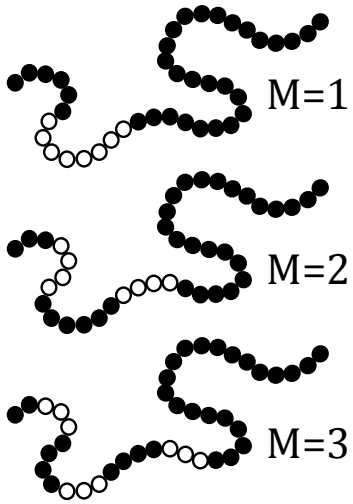

Figure 6.9: Schematics of the chains used to approximate the $A/B-A$ random copolymers. M is the number of ABA triblocks composing the random chain.

6.2.1 The Order-Disorder Transiton

First, we will use the random phase approximation to examine the effects of blockiness and polydispersity on the ODT. It will be necessary two define two ensembles of segments: the ABA triblocks composing the random chain, and the A-blocks composing

the homopolymer. This means that equation 2.31, which was previously derived for a chain composed of two separate random copolymers, can be used to give the inverse structure factor. This scenario turns out to be much simpler than the general case because the average profiles of the homopolymer are simply given by,

$$\begin{aligned}\langle g_A(s)\rangle &= 1,\\ \langle g_B(s)\rangle &= 0,\\ \langle g_{AA}(s,s')\rangle &= 1,\\ \langle g_{AB}(s,s')\rangle &= 0,\\ \langle g_{BB}(s,s')\rangle &= 0,\end{aligned}$$

which means that several of the correlation function components do not need to be calculated.

Previously, it was seen that the ODT of a random copolymer melt is approximately inversely proportional to the blockiness. In the limiting case, as M becomes large (or as the segments become small), the chain has the characteristics of a simple alternating copolymer. In the limiting case with $A/B-A$ random copolymers, the random chain becomes like a alternating copolymer, but the large A homopolymer remains. Thus, the chain as a whole bears more of a resemblance to a diblock. It would be expected then that the asymptotic behaviour of the ODT would not be a direct proportionality to M (i.e $\chi_c \sim M$), but would instead approach a constant value.

The critical point was calculated using the RPA as a function of M using both symmetric triblocks and asymmetric triblocks. As expected, the critical point quickly

levels off as M grows, but at different rates depending on the distribution width β.

For a lone random polymer, it was found that the effects of randomness become more significant as M is increased, due to the fact that the critical point approaches a straight line whose slope is diminished by increasing β. Now, because all the spinodal curves approach the same value, increasing M does not augment the effect, but appears to diminish it. In the case of symmetric triblocks with compositional dispersity, increasing the randomness was again seen to decrease the critical point, but to nowhere near the extent previously observed (Figure 6.10a). Also, there is no macrophase separation, which was seen to occur for a lone copolymer with with high compositional dispersity. Comparing this to the case of asymmetric compositionally monodisperse triblocks, there is a slight decrease in the critical point, but the effect is virtually negligible (Figure 6.10b).

6.2.2 Effects of Polydispersity on the Complete Phase Behaviour

The full phase behaviour was calculated using SCFT for $M = 1, 2, ..., 5$, first using the single-chain approximation (i.e. with $\beta = 1$), and then using low polydispersity ($\beta = 0.9$) and high polydispersity ($\beta = 0.8$) for both the symmetric and asymmetric triblock ensembles. The critical point is found with RPA. For $M = 1$ and $M = 2$, the sequence space is small enough that the integral was performed in full (requiring 9 and 81 MDE's respectively). For $M \geq 3$, the sequence space was too large to test entirely so the multi-chain approximation shown in section 2.3.2 was employed with $S = 100$.

Shown in Figure 6.11 is the phase behaviour of $A/B - A$ copolymers with $\beta = 1$.

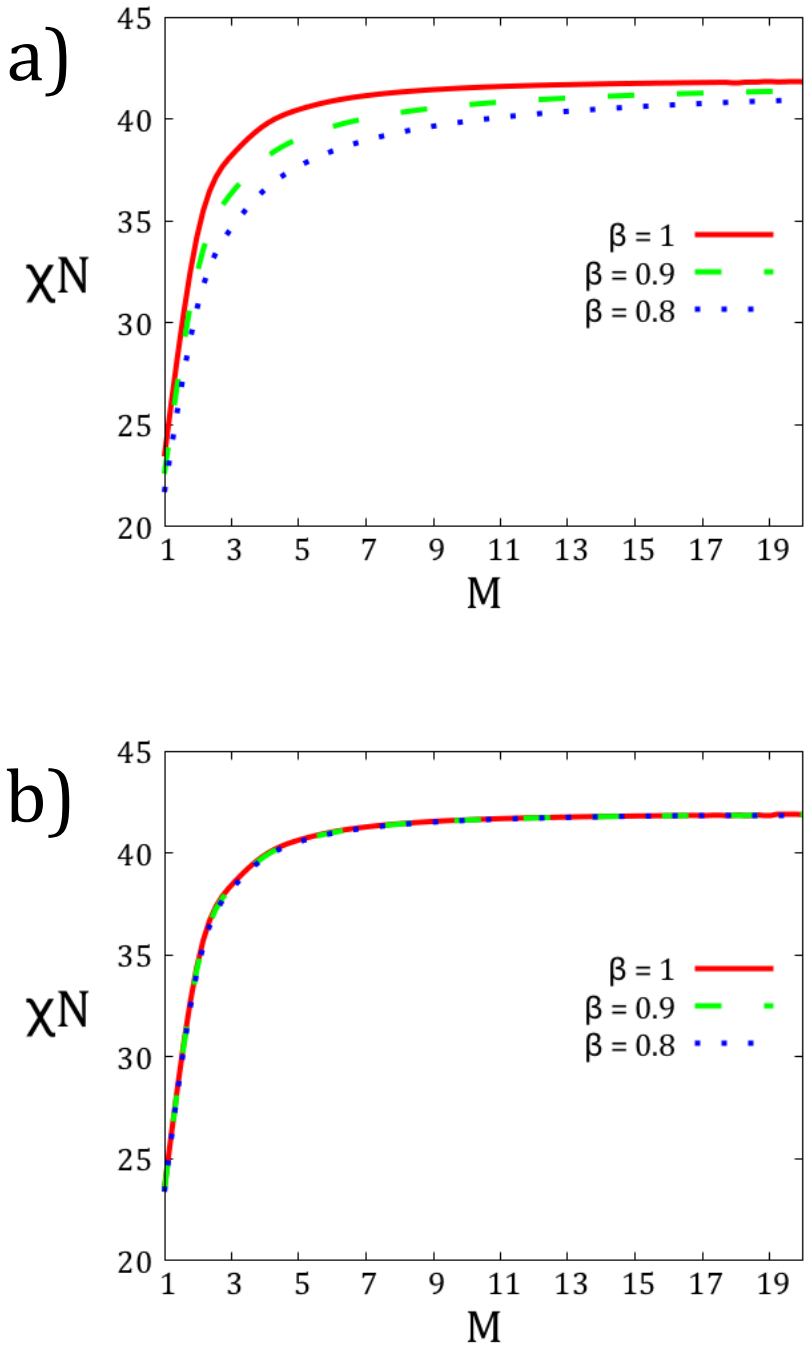

Figure 6.10: a) The critical point of $A/B-A$ random copolymers using the symmetric triblock segment ensemble plotted over a range of blockiness M and distribution width β; b) The critical point of $A/B-A$ random copolymers using the asymmetric triblock segment ensemble plotted over a range of blockiness M and distribution width β.

The hierarchical lamellar structures are labelled lam_n where n is the number of B layers within one period of the structure. lam_d refers to the simple lamellar structure. It is seen that non-lamellar structures are stable only for $M = 1$, and that as M grows, different hierarchical lamellar structures become stable. The simple lamellar appears only in the regime of $A/B-A$ domain ordering. The transition point between $A/B-A$ and AB domain ordering was calculated by the condition $\frac{d^2\psi}{d\chi^2} = 0$ as was described in section 4. Interestingly, this transition appears to be a linear function of M, in the same way that the critical point was for pure random copolymers.

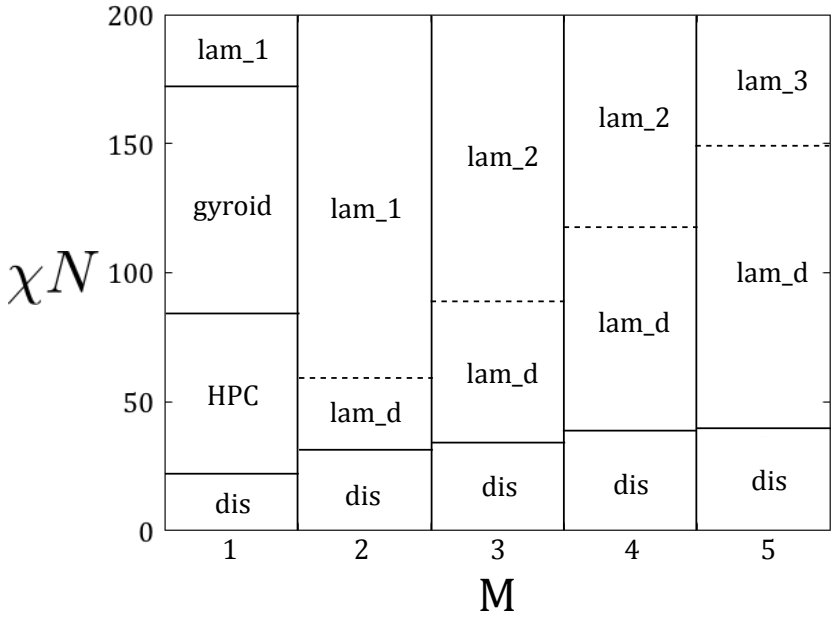

Figure 6.11: Full phase behaviour of $A/B - A$ random copolymers using symmetric triblocks with $\beta = 1$.

Turning now to the phase behaviour with the inclusion of compositional polydispersity (Figures 6.12, 6.13), we see that the most dramatic change in phase behaviour occurs for $M = 1$. In particular, the HPC structure becomes favoured over the gyroid and lamellar. By $\beta = 0.8$, the HPC dominates entirely. Beyond $M = 1$, the

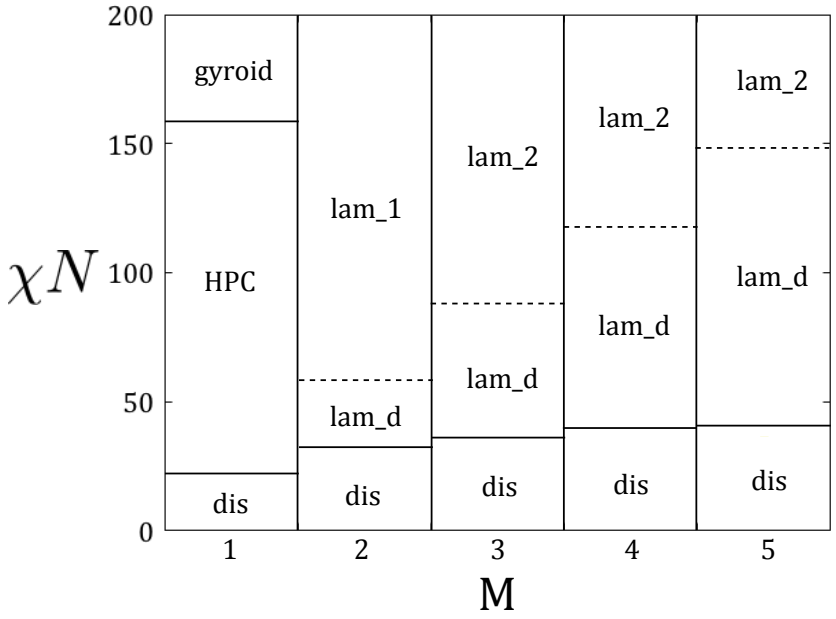

Figure 6.12: Full phase behaviour of $A/B-A$ random copolymers using symmetric triblocks with $\beta = 0.9$.

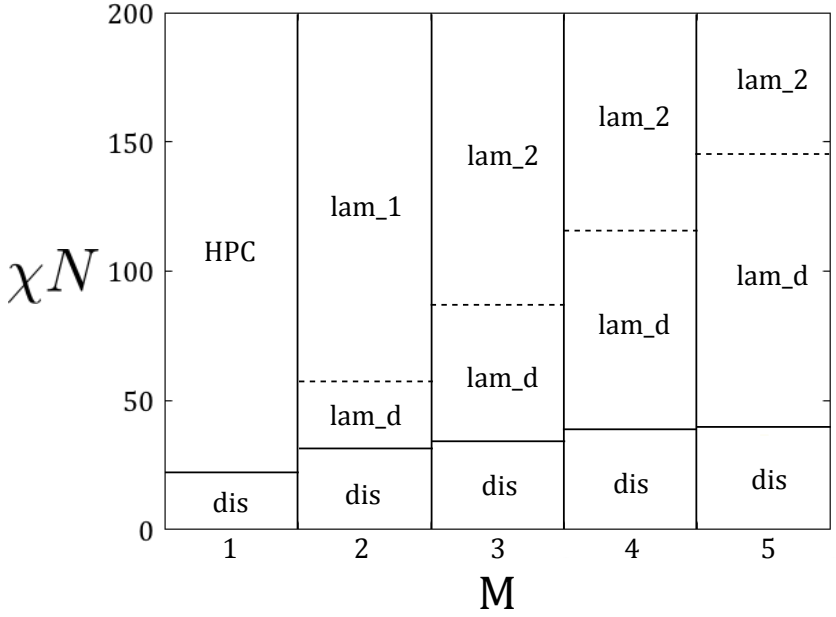

Figure 6.13: Full phase behaviour of $A/B-A$ random copolymers using symmetric triblocks with $\beta = 0.8$.

effect is less pronounced. The $A/B - A \rightarrow AB$ transition is negligibly affected, and only lamellar structures are seen beyond $M = 1$. The particular hierarchical lamellar structure is seen to be affected by polydispersity. The lam_3 structure, stable for $M = 5$ and $\beta = 1$, becomes lam_2. Because the HPC was stabilized so significantly in the $M = 1$ case, it is perhaps surprising that is does not appear anywhere else. Noting that the $M = 2$ integral was done in full, and that the HPC structure was unstable at this level of blockiness, we can be confident that the absence of HPC structures in the approximated $M > 2$ cases can be trusted, and is not an artifact of the approximation method. It is worth noting that even at $M = 5$ (which is a large sequence space), differences between the single-chain and multi-chain approximations are observed. This supports the idea that it is sufficient to survey the sequence space without integrating it entirely in order to see the effects of randomness on the phase behaviour.

Turning to pure sequential dispersity, we see first that the effect of the randomness on the phase behaviour is greatly diminished in comparison to the effect of compositional dispersity (Figures 6.14, 6.15). This is perhaps not surprising considering the negligible effect on the critical point that has already been shown. Interestingly, the effect on the phase behaviour, while more subtle, is also the 'reverse' of the effect of compositional dispersity. The HPC structure actually becomes slightly *less* stable compared to the gyroid and lamellar structures. Again the $A/B - A \rightarrow AB$ transition is negligibly affected. Beyond $M = 1$, there is no observed change in the phase behaviour.

Part of the purpose of these calculations is to evaluate the usefulness of the single-chain approximation. It is seen that the importance of randomness on the phase

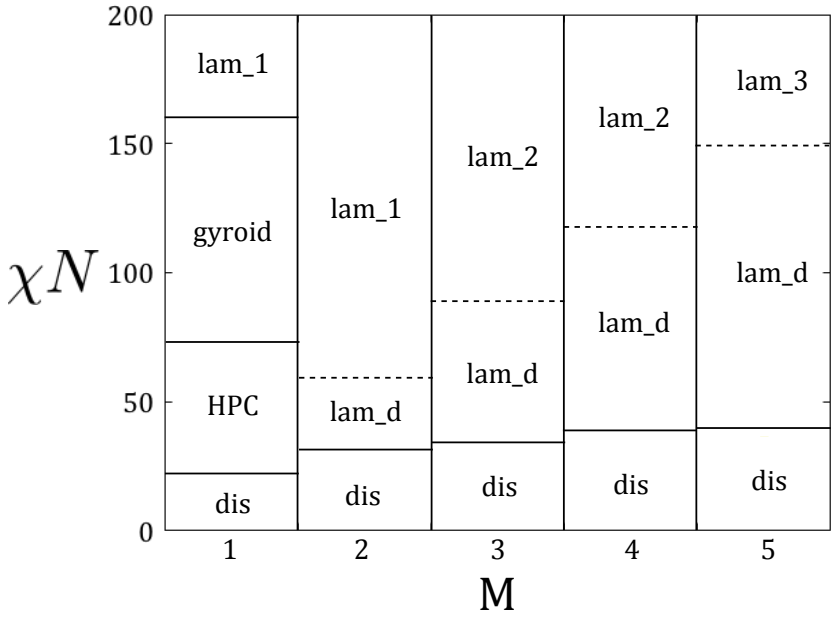

Figure 6.14: Full phase behaviour of $A/B-A$ random copolymers using asymmetric triblocks with $\beta = 0.9$.

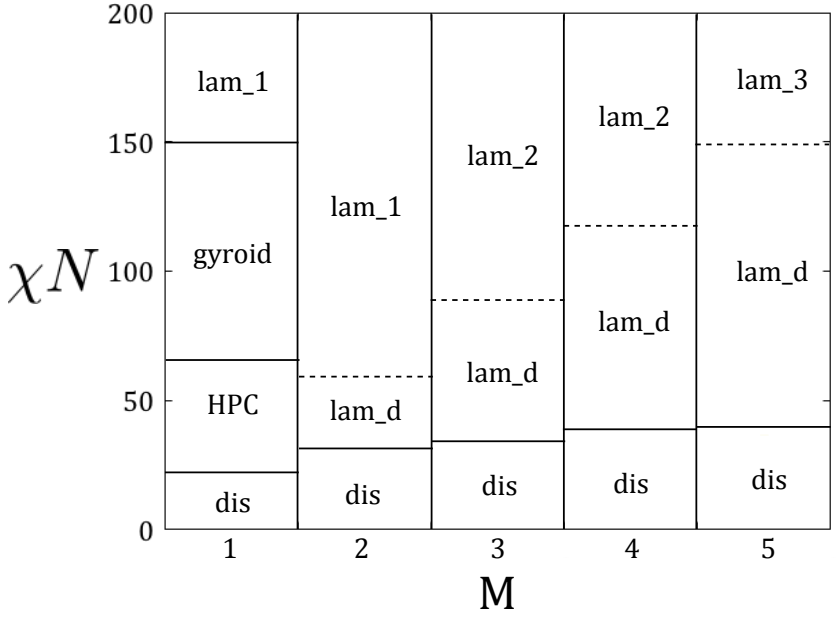

Figure 6.15: Full phase behaviour of $A/B-A$ random copolymers using asymmetric triblocks with $\beta = 0.8$.

behaviour depends strongly on the compositional variance of the melt. Even at high sequential dispersity, the single-chain approximation gives the correct sequence of transitions and reasonable good placement of where these transitions occur. As M gets larger, there is no discernible discrepancy between the two methods. With compositional dispersity, the effect is much more significant and the single-chain approximation becomes less accurate. However, for $M > 1$, the agreement is still quite good. The single-chain approximation depends on the idea that blockiness is the dominant characteristic that governs phase behaviour. It would appear from these results that blockiness alone is the most important characteristic if the compositional variance is low, but if the variance is high, both need to be taken into account. It would appear then, as a practical matter, that for a melt of random copolymers with low compositional variance, a single-chain approximation is likely sufficient, but that if variance is high, then the sequence space integral needs to be included in some form.

Previous work has been done on the problem of including polydispersity in SCFT; in particular, length polydispersity. Sides and Fredrickson introduced a method which approximates the integral using Gaussian quadrature [18]. In this application, the integral ranges from 0 to ∞, which makes using equally spaced points less sensible. It would be possible to apply such a scheme to the integrals used here to reduce the number of points per dimension S. However, the cost will still grow exponentially with M. Incorporating this method may increase the maximum M beyond which a different approximation would be necessary. Alternatively, Cooke and Shi developed a perturbation theory for polydisperse diblock copolymers and incorporated it into the spectral SCFT [34]. This approach has already been used to examine the effects of compositional polydispersity on gradient copolymers [7]. Within the segment model,

a function of the chain parameters $f(\{n\})$ can be expanded as,

$$\langle f(\{n\})\rangle \approx f(\{\langle n\rangle\}) + \frac{1}{2}\sum_i \kappa_i \frac{\partial^2 f}{\partial n_i^2}\bigg|_{n_i=\langle n\rangle} . \tag{6.5}$$

This expansion is possible because of the statistical independence of the n_i parameters. The advantage of this approach is that there is that the computational cost no longer grows exponentially in M. However, because this is a perturbation method, the polydispersity should be small. The advantage of Fredrickson and Sides' approach is that large degrees of polydispersity can be accommodated. If β is small, is may be that a single-chain approximation is sufficient. However, if these calculations were to be done on pure random copolymers, by which I mean random copolymers without the large A homopolymer block, the effects of polydispersity are likely to be more significant. Incorporating a perturbation method into the segment model for those systems would likely be a useful addition to the theoretical framework so far developed.

6.3 Phase Behaviour of PSS-PMB

A practical example of random copolymer whose sequence is not governed by Markov statistics is poly(styrenesulfonate-b-methylbutylene) (PSS-PMB). PSS-PMB is a diblock copolymer of PS-PMB in which a random selection of PS monomers have been sulfonated post-polymerization. Studies on this polymer, both by experiments and by Monte Carlo (MC) simulations, have shown that it displays interesting phase behaviour. In particular, a melt of symmetric PSS-PMB has a stable gyroid morphology with channels that occupy 50% of the total volume of the structure [35, 36, 37, 38]. This morphology has been termed a 'swollen gyroid' [38]. The equivalent, un-sulfonated polymer would only form the lamellar structure. In this section, we use self-consistent field theory to investigate the effects of blockiness on the phase behaviour of this polymer. The parameters are borrowed from [35] in order to allow a direct comparison to the MC results. The PS monomers will be labelled with subscript A, the PSS monomers with subscript B, and the PMB monomers with subscript C. The total volume fractions of the different components are,

$$f_A = 0.29$$

$$f_B = 0.21$$

$$f_C = 0.5$$

with Flory-Huggins parameters,

$$\chi_{AB} = \chi$$
$$\chi_{AC} = 0.042\chi$$
$$\chi_{BC} = 0.792\chi.$$

The $A/B{-}C$ random copolymers are implemented into the segment model by treating the A/B block as a series of M symmetric ABA triblocks. Because we are primarily interested in the phase behaviour as a function of M, we will use the single chain approximation with $\beta = 1$.

6.3.1 $A/B - C \rightarrow ABC$ Transition

In the previous section, it was seen that $A/B{-}C$ random copolymers can have diblock or multiblock copolymer characteristics depending on the blockiness of the random chain and the strength of the interactions. This difference is seen in whether the ordered phase consists of separate A, B, and C domains, or of a 'disordered' A/B domain and C domain. Using the order parameter $\psi(\chi)$ as defined in section 4, a general phase diagram was calculated for PSS-PMB (Figure 6.17). As before, it is seen that the ODT approaches a constant value as the diblock-like nature of the polymer becomes dominant. As well, the $A/B - C \rightarrow ABC$ boundary is approximately proportional to M.

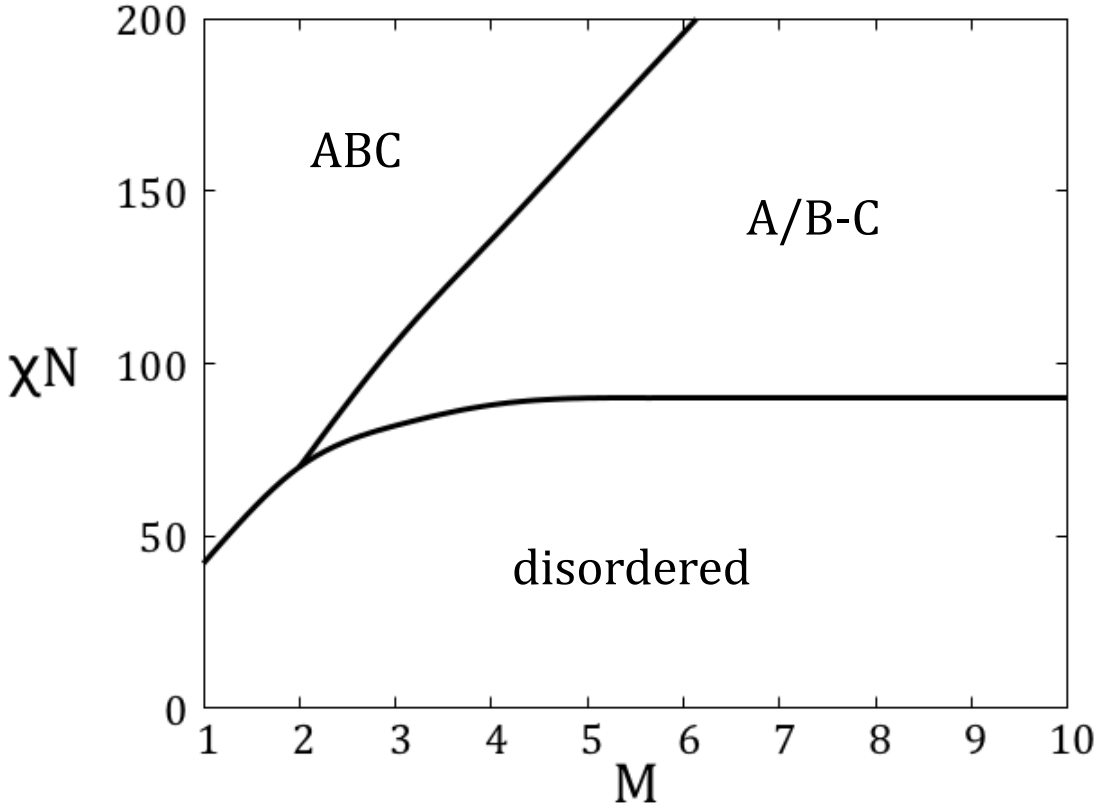

Figure 6.16: General phase behaviour of a monodisperse melt of PSS-PMB. Note that M is a discrete variable, the lines are provided to guide the eye.

6.3.2 Effects of Blockiness on the Phase Behaviour

The full phase behaviour was calculated for $M = 1, 2, ..., 10$ (Figure 6.17. Candidate structures included the usual diblock morphologies as well as hierarchical lamellar and HPC structures. The results are be in good agreement with the results of MC simulations. In particular, the same series of phase transitions for the case $M = 1$ was predicted by both MC simulations and SCFT (disordered $\rightarrow$ HPC $\rightarrow$ gyroid $\rightarrow$ lamellar). Due to computational constraints, we limit our window of observation to $\chi N < 200$. In this region, it was found that a grid resolution of at least 64x was necessary to get an accurate gyroid free energy. Extrapolating our results gives a predicted gyroid/lamellar transition at about $\chi N = 240$.

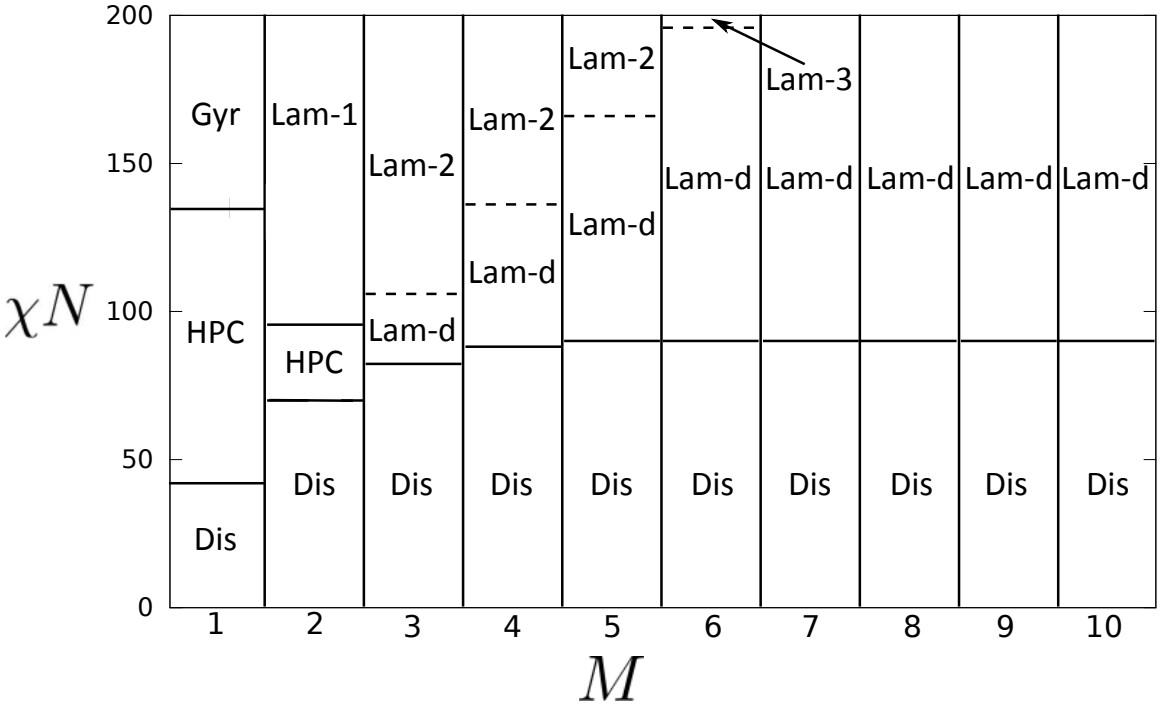

Figure 6.17: Complete phase behaviour of a monodisperse melt of PSS-PMB

A discrepancy between SCFT and MC results occurs at $M = 2$. MC simulations

predict a gyroid/lamellar transition (Figure 9*a* in [35]) while SCFT predicts an HPC/lamellar transition. Because of this discrepancy, and because the most dramatic change in phase behaviour occurs between $M = 1$ and $M = 2$, we take a closer look at the phase behaviour in this region by using a binary blend of $M = 1$ and $M = 2$ polymers to approximate an intermediate case (Figure 6.18).

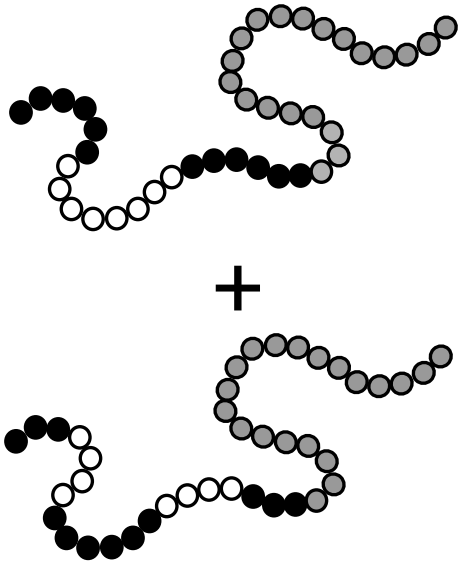

Figure 6.18: Schematic of the $M = 1$ and $M = 2$ PSS-PMB polymers used in a blend to evaluate the phase behaviour with intermediate blockiness

The 'blend fraction' is defined as the proportion of chains of type $M = 2$. Therefore a fraction of 0 corresponds to a monodisperse melt of $M = 1$ polymers while a fraction of 1 corresponds to a monodisperse melt of $M = 2$ polymers. As the blend fraction increases (or as the blockiness decreases), the gyroid structure becomes displaced by the lamellar structure. The HPC structure is also destabilized but not to the same extent. There is a triple point at $\chi N = 95$ when the blend fraction is 87.5%. Beyond this point, the gyroid is unstable for any χN leaving only the HPC and lamellar structures.

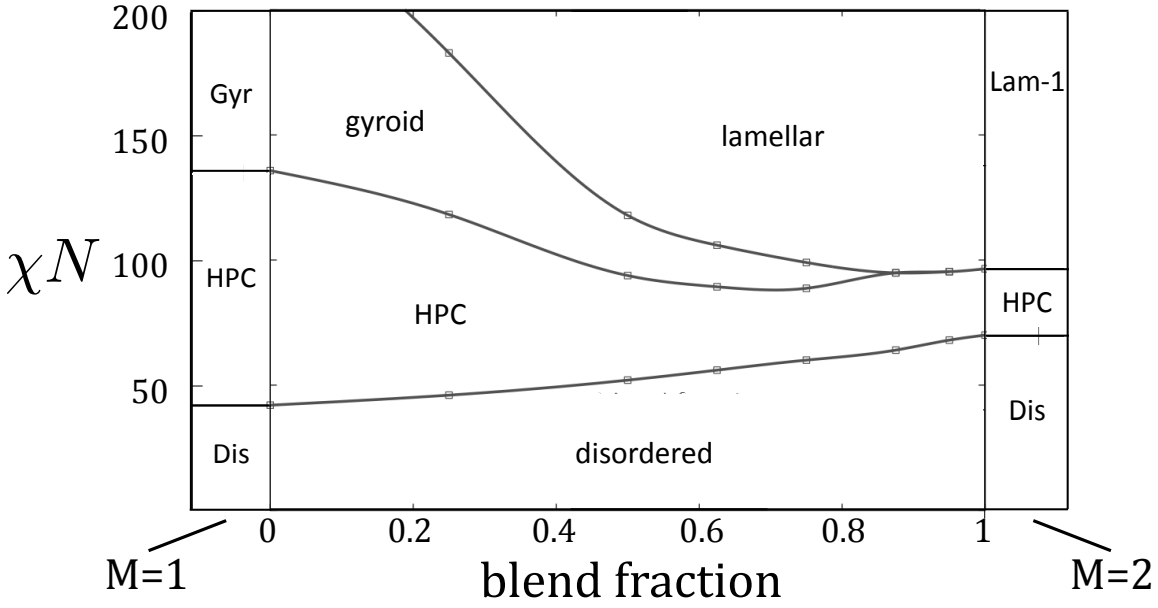

Figure 6.19: Phase behaviour of a binary blend of $M = 1$ and $M = 2$ PSS-PMB. The blend fraction is defined as the fraction of polymers of type $M = 2$.

6.3.3 Substructure of the Swollen Gyroid

From $M = 1$ to $M = 2$, the phase behaviour is exclusively of type ABC. The random chain forms a core-shell substructure with the PSS monomers forming the core while the PS monomers for the shell. For example, the substructure of the HPC morphology is shown in Figure 6.20. The gyroid structure is particularly interesting in this case because it appears to be a gyroid with a volume fraction of 50%, in sharp contrast to the usual 30% at which the gyroid is stable for simple a block copolymer. This particular gyroid morphology has been previously termed a 'swollen gyroid'. As with the HPC, the gyroid formed by PSS-PMB has an extra level of organization from the usual gyroid consisting of a PSS-PS core-shell substructure. Because the PS monomers form a shell around the PSS gyroid channels, it is not completely unambiguous to state that this gyroid has a volume fraction of 50%. If we

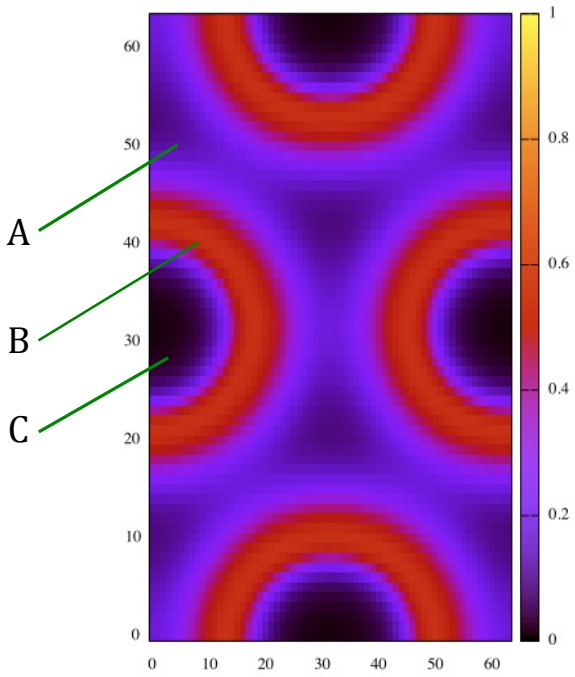

Figure 6.20: Core-shell substructure of the HPC phase. Plotted is the local concentration of PS monomers. A) PMB matrix, B) PS shell, C) PSS core.

view the PS/PSS random chain as a single unit then this is certainly true; a gyroid is stable while the equivalent symmetric diblock copolymer would only form the lamellar structure. On the other hand, the channels themselves do not have a volume fraction of 50%. Plotting the local concentration of a slice of the swollen gyroid, it is clear that the PSS monomers form the usual channel pattern, but that the PS monomers not only sheath the channels but connect them (Figure 6.21). It is questionable to state that this structure is a 50% volume fraction *gyroid*. The two components that together form the 50% are arranged differently within the structures; the PS monomers form distinct channels within one continuous substructure while the PS monomers form a sub-matrix in which the channels are embedded. Note that in the core-shell HPC structures, the cylinders remain entirely distinct, even if the PS and PSS components are taken together as a single unit. The PSS monomers in this case can be less ambiguously said to compose the cylinders and not the matrix. Because in the case of the gyroid taking the PS and PSS monomers as a single unit makes the channels no longer distinct, it is uncertain that the PS shell can be properly said to compose channels anymore than the equal volume PMB matrix can be said to compose channels. Rather, it may be that this particular swollen gyroid morphology is best described as a core-shell double gyroid with a channel volume fraction of 21%. For the sake of comparison, I would refer readers to the core-shell double gyroid formed by poly(isoprene-b-styrene-b-dimethylsiloxane) as shown in [39]. The authors referred to this structure as a pentacontinuous phase because it features two distinct channels, two distinct shells, and one matrix. This structure has channel, shell and matrix volume fractions 0.19, 0.41, and 0.40 respectively. This structure is technically designated a pentcontinuous phase, instead of a bicontinuous phase, because the

isoprene, styene, and dimethylsiloxane are viewed as purely distinct components. Because of the inherently random nature of $PSS-PMB$, it is not as easy to separate the PS and PMB. However, SCFT and MC simulation agree that only the blockiest $PSS-PMB$ sequences can form the swollen gyroid, implying that phase separation within the random chain is key to the stability of this structure. If this is true, then it is possible that this gyroid is not a bicontinuous phase with volume fraction 0.5, but a pentacontinuous phase with channel, shell, and matrix volume fractions 0.21, 0.29, and 0.5 respectively.

It is important at this point to make clear the context of these calculations and the extent to which they may be compared to the previously mentioned Monte Carlo simulations. Within that collection of research, two distinct classes of morphologies were observed. One is where the A/B block forms the structure while the C block forms the matrix. The other is where the C block forms the structure while the A/B block forms the matrix. The context in which the term 'swollen gyroid' originated was from a set of simulations in which the channels were seen to be formed by the C block [37, 38]. The gyroid studied here, though also with an apparent volume fraction of 50%, is the 'reverse' situation. As such, it must be stressed that these calculations refer to the particular gyroid observed in reference [35]. In those simulations, as in these calculations, the chain architecture was commensurate with a core-shell morphology. Later simulations reversed this block ordering, now embedding A blocks within a large B block. In our model, this would be equivalent to using BAB triblocks instead of ABA triblocks. This change in block ordering introduces a level of frustration which, at least in the MC simulations, has a significant effect on the ordered phase. Although our calculations give a clue that substructure within

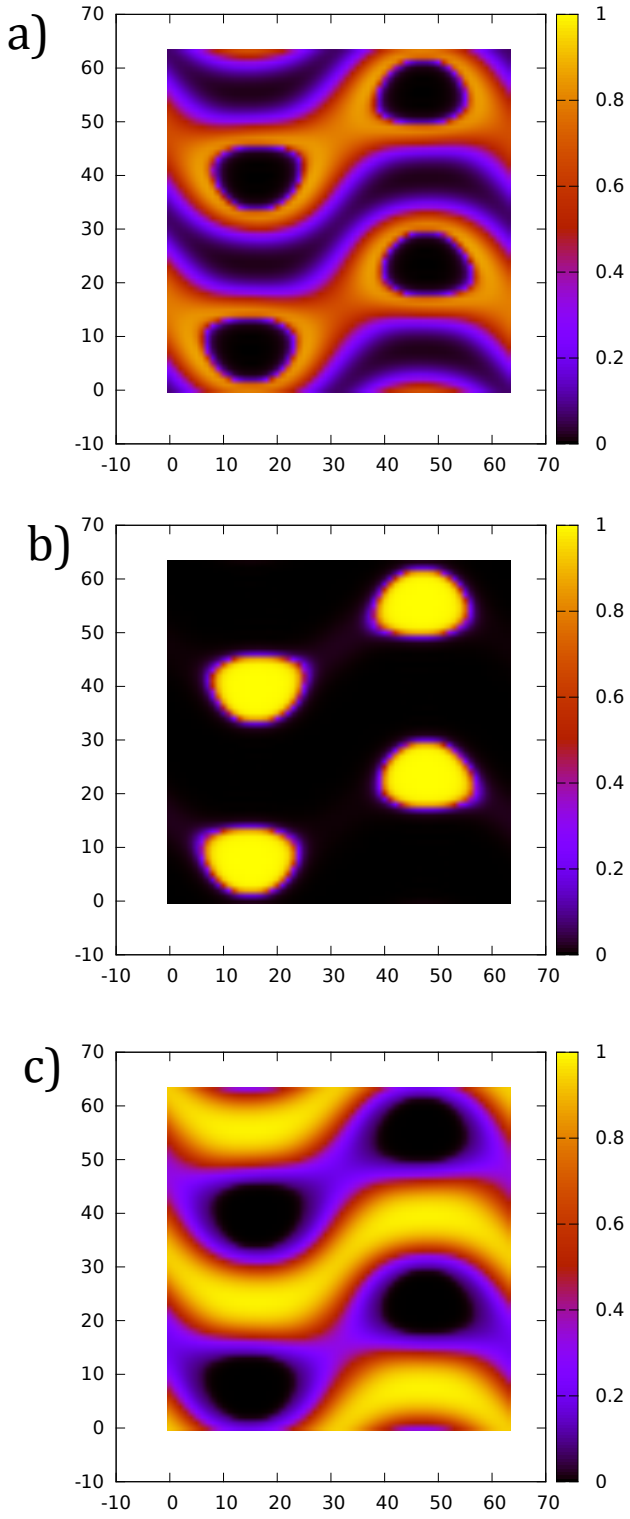

Figure 6.21: Core-shell substructure of the swollen gyroid phase. Plotted are the local monomer concentrations of a slice of the structure a) PS monomers, b) PSS monomers, c) PMB monomers

the A/B domain is a key to the gyroid's stability, it may be that the core-shell morphology is stable only for the case where the chain architecture is not frustrated. In order to complete the SCFT analysis of this structure and to compare directly to more recent MC simulations, it will be necessary to repeat these calculations using BAB triblocks.

Chapter 7

Conclusions and Outlook

In this thesis, a model for describing random block copolymers in the context of blockiness is developed and analyzed using the Random Phase Approximation and Self-Consistent Field Theory. In the model each chain is composed of M equal length segments whose individual sequences are drawn from some distribution. The blockiness is controlled by the number of segments M, while the randomness is introduced through the ensemble of segments $g_\alpha(n, s)$ and the associated distribution $P(n)$. The model was implemented into the random phase approximation and it was seen that the computational cost of RPA calculations for the model is independent of the dimensionality of the sequence space. This result is general and makes no restrictions with respect to the nature of the segments, apart from the assumptions of equal length and statistical independence (i.e $P(n, n') = P(n)P(n')$). Because of this generality, it is possible to extend this model to other specific chain architectures such as a random block copolymer joined to a homopolymer, or perhaps to more complicated melts such as a blend of two distinct types of random copolymers. It is also possible to extend the model to include variability in M.

It was generally observed that the critical point approaches a linear relation to M, therefore the critical point is inversely proportional to the blockiness. Increasing the variability among the chains, both compositionally and sequentially, was seen to not alter this trend, but will reduce the slope of this linear relation. It was shown that in the regime of macrophase separation, the critical point is determined entirely by the compositional variance of the system. Macrophase separation was only observed to occur with sufficiently high compositional variance, thus sequential variability can facilitate microphase separation but will not drive macrophase separation.

Extending the model to SCFT is straightforward, but with substantial computational cost. Solving the SCFT equations requires integrating the partition function over the sequence space. If the integral is approximated as a sum, each term bringing with it an additional MDE, the number of MDE's the need to be solved rises exponentially with the dimension of the sequence space. This was not an issue with the RPA implementation because the different segments can be treated as independent of each another. In the case with SCFT however, the propagator at any contour position s depends explicitly on every contour position that preceded it. Doing the full calculation is only practical for the smallest values of M, particularly if 3-dimensional morphologies are among the candidate structures. Two approximation methods were suggested and demonstrated in this work. The first is a single-chain approximation which ignores randomness entirely and treats the system as a monodisperse melt. Our results indicate that this method may be appropriate if the compositional variance is small. A compositionally monodisperse blend, even with high sequential polydispersity was well described by the single-chain approximation. It is particularly useful if the sequence of phase transitions is the primary object of interest. The second

method is a multi-chain approximation in which an ensemble of chains are generated randomly and used to represent the entire melt. Other approaches were suggested that would be worth exploring in future work. In particular, it would be an improvement over the single-chain approximation to implement a perturbation method into the segment model, in the manner done in [34].

The single-chain approximation was used to study the effects of blockiness on the phase behaviour of $PSS - PMB$. The SCFT results were consistent with previous experiments and MC simulations, with some discrepancy with regard to the stability of the gyroid phase. MC simulations predict that as the blockiness of the random chain decreases, the HPC structure vanishes before the gyroid. SCFT calculations suggest that while decreases in the blockiness destabilized both phases, the gyroid vanishes first. This trend was examined more closely by using a binary blend of $M = 1$ and $M = 2$ chains to simulate intermediate levels of blockiness, and the gradual disappearance of the gyroid was observed. In addition, the gyroid was found to consist of a core-shell substructure, similar to the pentacontinuous gyroid observed in poly(isoprene-b-styrene-b-dimethylsiloxane). The gyroid increases in stability as the blockiness increases, indicating the phase separation within the random chain is an important factor of its stability. This is supported by both SCFT and MC simulations. A complete analysis of this system will require additional calculations using a frustrated chain architecture not conducive to the core-shell arrangement. This will allow for direct comparison to a wider range of MC simulations. For future work on this topic, it would be useful to move beyond the single-chain approximation and examine the effects of compositional and sequential variability on the stability of this structure. The SCFT calculations on the $A/B - A$ random copolymer, which is

similar to PSS-PMB, indicates that while compositional variability may destabilize the gyroid in favour of the HPC phase, sequential variability may actually increase its stability.

Bibliography

[1] F. S. Bates, M. A. Hillmyer, T. P. Lodge, C. M. Bates, K. T. Delaney, and G. H. Fredrickson, "Multiblock polymers: Panacea or pandora's box?," *Science*, vol. 336, no. 6080, pp. 434–440, 2012.

[2] J.-F. Lutz, "Aperiodic copolymers," *ACS Macro Lett*, vol. 3, no. 10, pp. 1020–1023, 2014.

[3] G. H. Fredrickson and S. T. Milner, "Thermodynamics of random copolymer melts," *Phys. Rev. Lett.*, vol. 67, pp. 835–838, Aug 1991.

[4] G. H. Fredrickson, S. T. Milner, and L. Leibler, "Multicritical phenomena and microphase ordering in random block copolymers melts," *Macromolecules*, vol. 25, no. 23, pp. 6341–6354, 1992.

[5] C. D. Sfatos, A. M. Gutin, and E. I. Shakhnovich, "Phase diagram of random copolymers," *Phys. Rev. E*, vol. 48, pp. 465–475, Jul 1993.

[6] M. J. Park and N. P. Balsara, "Phase behavior of symmetric sulfonated block copolymers," *Macromolecules*, vol. 41, no. 10, pp. 3678–3687, 2008.

[7] R. Jiang, Z. Wang, Y. Yin, B. Li, and A.-C. Shi, "Effects of compositional polydispersity on gradient copolymer melts," *J. Chem. Phys*, vol. 138, no. 7, 2013.

[8] R. Jiang, Q. Jin, B. Li, D. Ding, R. A. Wickham, and A.-C. Shi, "Phase behavior of gradient copolymers," *Macromolecules*, vol. 41, no. 14, pp. 5457–5465, 2008.

[9] G. V. Z. Schulz, "The molecular weight distribution of oligomers," *J. Phys. Chem*, vol. B43, p. 25, 1939.

[10] L. Leibler, "Theory of microphase separation in block copolymers," *Macromolecules*, vol. 13, no. 6, pp. 1602–1617, 1980.

[11] A. Aksimentiev and R. Hoyst, "Phase behavior of gradient copolymers," *J. Chem. Phys*, vol. 111, no. 5, 1999.

[12] V. Ganesan, N. A. Kumar, and V. Pryamitsyn, "Blockiness and sequence polydispersity effects on the phase behavior and interfacial properties of gradient copolymers," *Macromolecules*, vol. 45, no. 15, pp. 6281–6297, 2012.

[13] M. W. Matsen, "The standard gaussian model for block copolymer melts," *J. Phys. Condens. Matter*, vol. 14, no. 2, p. R21, 2002.

[14] V. G. Glenn H. Fredrickson and F. Drolet, "Field-theoretic computer simulation methods for polymers and complex fluids," *Macromolecules*, vol. 35, no. 1, pp. 16–39, 2002.

[15] F. Schmid, "Self-consistent-field theories for complex fluids," *J. Phys. Condens. Matter*, vol. 10, p. 8105, 1998.

[16] A.-C. Shi, "Self-consistent field theory of block copolymers," in *Developments in Block Copolymer Science and Technology* (I. Hamley, ed.), ch. 8, New York: John Wiley & Sons, 2004.

[17] M. W. Matsen, "Effect of large degrees of polydispersity on strongly segregated block copolymers," *Eur. Phys. J. E*, vol. 21, no. 3, pp. 199–207, 2006.

[18] S. W. Sides and G. H. Fredrickson, "Continuous polydispersity in a self-consistent field theory for diblock copolymers," *J. Chem. Phys*, vol. 121, no. 10, pp. 4974–4986, 2004.

[19] D. M. Cooke and A.-C. Shi, "Effects of polydispersity on phase behavior of diblock copolymers," *Macromolecules*, vol. 39, no. 19, pp. 6661–6671, 2006.

[20] M. W. Matsen and M. Schick, "Stable and unstable phases of a diblock copolymer melt," *Phys. Rev. Lett.*, vol. 72, pp. 2660–2663, Apr 1994.

[21] K. Rasmussen and G. Kalosakas, "Improved numerical algorithm for exploring block copolymer mesophases," *J. Polym. Sci. Part B Polym. Phys.*, vol. 40, no. 16, pp. 1777–1783, 2002.

[22] M. W. Matsen, "Fast and accurate scft calculations for periodic block-copolymer morphologies using the spectral method with anderson mixing," *Eur. Phys. J. E*, vol. 30, no. 4, pp. 361–369, 2009.

[23] A. Ranjan, J. Qin, and D. C. Morse, "Linear response and stability of ordered phases of block copolymer melts," *Macromolecules*, vol. 41, no. 3, pp. 942–954, 2008.

[24] E. W. Cochran, C. J. Garcia-Cervera, and G. H. Fredrickson, "Stability of the gyroid phase in diblock copolymers at strong segregation," *Macromolecules*, vol. 39, no. 7, pp. 2449–2451, 2006.

[25] G. H. Weiss and A. A. Maradudin, "The bakerhausdorff formula and a problem in crystal physics," *J. Math. Phys.*, vol. 3, no. 4, 1962.

[26] R. B. Thompson, K. O. Rasmussen, and T. Lookman, "Improved convergence in block copolymer self-consistent field theory by anderson mixing," *J. Chem. Phys*, vol. 120, no. 1, 2004.

[27] P. Stasiak and M. W. Matsen, "Efficiency of pseudo-spectral algorithms with anderson mixing for the scft of periodic block-copolymer phases," *Eur. Phys. J. E*, vol. 34, no. 10, pp. 1–9, 2011.

[28] K. Jiang, J. Zhang, and Q. Liang, "Self-assembly of asymmetrically interacting abc star triblock copolymer melts," *J. Polym. Sci. Part B Polym. Phys.*, vol. 119, no. 45, pp. 14551–14562, 2015.

[29] W. Li and A.-C. Shi, "Theory of hierarchical lamellar structures from a(bc)nba multiblock copolymers," *Macromolecules*, vol. 42, no. 3, pp. 811–819, 2009.

[30] W. Selke in *Phase Transitions and Critical Phenomena* (C. Domb and J. Lebowitz, eds.), vol. 15, Academic Press, 1992.

[31] M. W. Matsen and M. Schick, "Stable and unstable phases of a diblock copolymer melt," *Phys. Rev. Lett.*, vol. 72, pp. 2660–2663, Apr 1994.

[32] M. W. Matsen and R. B. Thompson, "Equilibrium behavior of symmetric aba triblock copolymer melts," *J. Chem. Phys*, vol. 111, no. 15, pp. 7139–7146, 1999.

[33] A. Subbotin and A. Semenov, "Phase equilibria in random multiblock copolymers," *Eur. Phys. J. E*, vol. 7, no. 1, pp. 49–64, 2002.

[34] D. M. Cooke and A.-C. Shi, "Effects of polydispersity on phase behavior of diblock copolymers," *Macromolecules*, vol. 39, no. 19, pp. 6661–6671, 2006.

[35] P. Knychala, M. Banaszak, M. J. Park, and N. P. Balsara, "Microphase separation in sulfonated block copolymers studied by monte carlo simulations," *Macromolecules*, vol. 42, no. 22, pp. 8925–8932, 2009.

[36] P. Knychala, M. Dzicielski, M. Banaszak, and N. P. Balsara, "Phase behavior of ionic block copolymers studied by a minimal lattice model with short-range interactions," *Macromolecules*, vol. 46, no. 14, pp. 5724–5730, 2013.

[37] P. Knychala, M. Banaszak, and N. P. Balsara, "Effect of composition on the phase behavior of ion-containing block copolymers studied by a minimal lattice model," *Macromolecules*, vol. 47, no. 7, pp. 2529–2535, 2014.

[38] P. Knychała and M. Banaszak, "Simulations on a swollen gyroid nanostructure in thin films relevant to systems of ionic block copolymers," *Eur. Phys. J. E*, vol. 37, no. 7, pp. 1–8, 2014.

[39] T. A. Shefelbine, M. E. Vigild, M. W. Matsen, D. A. Hajduk, M. A. Hillmyer, E. L. Cussler, and F. S. Bates, "Coreshell gyroid morphology in a poly(isoprene-block-styrene-block-dimethylsiloxane) triblock copolymer," *J. Am. Chem. Soc.*, vol. 121, no. 37, pp. 8457–8465, 1999.